Appears as pages 223-265 (Chapter 8) of Luigi Landini, Vincenzo Positano and Maria Filomena Santarelli (eds) *Advanced Image Processing in Magnetic Resonance Imaging*, Dekker, book series on Signal Processing and Communications, ISBN 0824725425, 2005.

# Chapter 8

# Multimodal Integration: fMRI, MRI, EEG, MEG

**Yaroslav O. Halchenko**[12] **Stephen José Hanson**[1] **Barak A. Pearlmutter**[3]

[1]*Psychology Dept., Rutgers-Newark, NJ 07102, USA*
[2]*Computer Science Dept., NJIT, Newark, NJ 07102, USA*
[3]*Hamilton Institute & Dept. of Computer Science, NUI Maynooth, Co. Kildare, Ireland*

*Revision: 1.220*

## Chapter Overview

This chapter provides a comprehensive survey of the motivations, assumptions and pitfalls associated with combining signals such as fMRI with EEG or MEG. Our initial focus in the chapter concerns mathematical approaches for solving the localization problem in EEG and MEG. Next we document the most recent and promising ways in which these signals can be combined with fMRI. Specifically, we look at correlative analysis, decomposition techniques, equivalent dipole fitting, distributed sources modeling, beamforming, and Bayesian methods. Due to difficulties in assessing ground truth of a combined signal in any realistic experiment—a difficulty further confounded by lack of accurate biophysical models of BOLD signal—we are cautious to be optimistic about multimodal integration. Nonetheless, as we highlight and explore the technical and methodological difficulties of fusing heterogeneous signals, it seems likely that *correct fusion* of multimodal data will allow previously inaccessible spatiotemporal structures to be visualized and formalized and thus eventually become a useful tool in brain imaging research.

## 8.1 Introduction

Non-invasive functional brain imaging has become an important tool used by neurophysiologists, cognitive psychologists, cognitive scientists, and other researchers interested in brain function. In the last five decades the technology of non-invasive functional imaging has flowered, and researchers today can choose from EEG, MEG, PET, SPECT, MRI, and fMRI. Each method has its own strengths and weaknesses, and no single method is best suited for all experimental or clinical conditions. Because of the inadequacies of individual techniques, there is increased interest in finding ways to combine existing techniques in order to synthesize the strengths inherent in each. In this chapter, we will: (a) examine specific non-invasive imaging techniques (EEG, MEG, MRI and

Table 8.1: *Notation used throughout this chapter.* We chose our notation to match the most popular conventions in the field, and at the same time minimize confusion. Regrettably, it is likely to differ from the notation used by each particular paper we reference. Following the usual conventions, we use bold upper case symbols for matrices, bold lower case for vectors, and non-bold symbols for scalars.

| Symbol | Meaning |
|---|---|
| $K$ | Number of simultaneously active voxels |
| $N$ | Number of voxels, *i.e.* spatial resolution of high spatial resolution modality (fMRI) |
| $M$ | Number of EEG/MEG sensors, *i.e.* spatial resolution of low spatial resolution modality |
| $T$ | Number of time points of high temporal resolution modality (EEG, MEG) |
| $U$ | Number of time points of low temporal resolution modality (fMRI) |
| $L$ | Number of orthogonal axes for dipole moment components, $L \in \{1, 2, 3\}$ |
| $\mathbf{I}_n$ | Identity matrix ($n \times n$) |
| $\mathbf{0}$ | Zero matrix of appropriate dimensionality |
| $\mathbf{X}$ | General E/MEG data matrix; can contain EEG or/and MEG data ($M \times T$) |
| $\mathbf{B}$ | BOLD fMRI data matrix ($N \times U$) |
| $\mathbf{Q}$ | Dipole sources matrix |
| $\mathcal{G}$ | General E/MEG lead function, incorporating information for EEG or/and MEG |
| $\mathbf{G}$ | General E/MEG lead matrix |
| $\mathbf{F}^i$ | Spatial filter matrix for the $i$-th dipole ($M \times L$) |
| $\nu$ | Variance |
| $\mathbf{C}$ | Covariance matrix |
| $\mathbf{K}$ | Matrix of correlation coefficients |
| $\mathbf{M}^\top$ | Matrix transpose |
| $\mathbf{M}^+$ | Generalized matrix inverse (pseudo-inverse) |
| $\operatorname{null} \mathbf{M}$ | The *null space* of $\mathbf{M}$, the set of vectors $\{\mathbf{x} \mid \mathbf{M}\mathbf{x} = 0\}$ |
| $\operatorname{diag} \mathbf{M}$ | The diagonal matrix with the same diagonal elements as $\mathbf{M}$ |

fMRI), (b) compare approaches used to analyze the data obtained from these techniques, and (c) discuss the potential for successfully combining methodologies and analyses.

Localizing neuronal activity in the brain, both in time and in space, is a central challenge to progress in understanding brain function. Localizing neural activity from EEG or MEG data is called *electromagnetic source imaging* (EMSI). EEG and MEG each provide data with high temporal resolution (measured in milliseconds), but limited spatial resolution. In contrast, fMRI provides good spatial but relatively poor temporal resolution. For some clinical purposes, or general localization, simple techniques can be used for source imaging. However, more specific localization of the neural activity requires more sophisticated analyses; for these, researchers turned to other disciplines that face similarly difficult localization problems (seismology, remote sensing, noninvasive signal processing, radar and sonar signal detection) for inspiration and algorithms. Because the source localization techniques used in EMSI serve as a starting point for subsequent multimodal analysis, we will discuss these methods first. We will review canonical problems of source localization, and how they have been attacked by various researchers.

Following this section we discuss problems inherent in multimodal experiments and then explore how MR modalities, which have high spatial resolution, can be combined with existing EMSI techniques in order to increase localization *precision* (for other reviews see George et al. (1995a); Nunez and Silberstein (2000); Salek-Haddadi et al. (2003); George et al. (2002)).

Demonstrated localization *accuracy* remains a distant goal confounded by the lack of ground truth in any

realistic experimental multimodal protocol and the lack of a complete model of the BOLD signal. Some progress on some very simple experiments where there is a small number of isolated focal sources of activity which are consistently present in all relevant modalities gives us hope that should be possible. We conclude that a convincing demonstration of increased accuracy for a complex protocol would constitute a major success in the field.

Throughout this chapter we provide a consistent and complete set of mathematical formulations that are stand alone, we also provide appropriate context for this notation into existing literature (Table 8.1 presents notation used throughout this chapter). Our conclusions and suggestions for future work make up the final section.

## 8.2 Source Localization in EEG and MEG

Electroencephalography (EEG) and magnetoencephalography (MEG) have been widely used in research and clinical studies since the mid-twentieth century. Although Richard Caton (1842–1926) is believed to have been the first to record the spontaneous electrical activity of the brain, the term EEG first appeared in 1929 when Hans Berger, a psychiatrist working in Jena, Germany, announced to the world that "it was possible to record the feeble electric currents generated on the brain, without opening the skull, and to depict them graphically onto a strip of paper." The first SQUID-based MEG experiment with a human subject was conducted at MIT by Cohen (1972) after his successful application of Zimmerman's SQUID sensors to acquire a magneto-cardiogram in 1969. EEG and MEG are closely related due to electro-magnetic coupling, and we will use E/MEG to refer generically to either EEG, MEG, or both altogether. E/MEG provides high temporal resolution (measured in milliseconds) but has a major limitation: the location of neuronal activity can be hard to determine with confidence. In the next section we lay out the specifics of each of the E/MEG signals, the premises for conjoint E/MEG analysis, and the EMSI techniques which have been adopted for use in multimodal analysis with fMRI data.

### 8.2.1 Assumptions Underlying Integration of EEG and MEG

The theory of electromagnetism and Maxwell's equations, under the assumption of quasi-stationarity[1], theoretically defines the relationship between observed magnetic and electric fields which are induced by the ionic currents generated inside the brain (see Malmivuo and Plonsey (1995); Okada et al. (1999); Murakami et al. (2003) for more information about the biophysics of E/MEG signals).

The similar nature of the EEG and MEG signals means that many methods of data analysis are applicable to both E/MEG modalities. Although the SNR of E/MEG signals have improved with technological advances, and some basic analysis has been performed by experts on raw E/MEG data via visual inspection of spatial signal patterns outside of the brain, more advanced methods are required to use data efficiently. During the last two decades many E/MEG signal analysis techniques (Michel et al., 2004) have been developed to provide insights on different levels of perceptual and cognitive processing of human brain: ERP (event related potential) in EEG and ERF (event related field) in MEG, components analysis (PCA, ICA, *etc.*), frequency domain analysis, pattern analysis, single-trial analysis (Jung et al., 1999b; Tang et al., 2000b; Tang and Pearlmutter, 2003), *etc.* Source localization techniques were first developed for MEG because the head model required for forward modeling of magnetic field is relatively simple. Source localization using an EEG signal has been difficult to perform since the forward propagation of the electric potentials is more complicated. However, recent advances in automatic MRI segmentation methods together with advances in forward and inverse EEG modeling, have made EEG source localization plausible.

[1] A signal is quasistatic if it does not change its parameters in time. The non-stationary term present in the E/MEG physical model is relatively small and can be considered zero in the range of signal frequencies which are captured by E/MEG. See Hämäläinen et al. (1993) for a more detailed description.

The theory of electromagnetism also explains why EEG and MEG signals can be considered complementary, in that they provide different views on the same physiological phenomenon (Wikswo et al., 1993; Hämäläinen et al., 1993; Cohen and Halgren, 2003). On one hand, often accented difference is that MEG is not capable of registering the magnetic field generated by the sources that are oriented radially to the skull surface in the case of spherical conductor geometry. On the other hand MEG has the advantage over EEG in that the local variations in conductivity of different brain matter (*e.g.* white matter, gray matter) do not attenuate the MEG signal much, whereas the EEG signal is strongly influenced by different types of brain matter and of the skull in particular (Okada et al., 1999). The orientation selectivity, combined with the higher depth precision due to homogeneity, make MEG optimal for detecting activity in sulci (brain fissures) rather than in gyri (brain ridges). In contrast, a registered EEG signal is dominated by the gyral sources close to the skull and therefore more radial to its surface. Yet another crucial difference is dictated by basic physics. The orthogonality of magnetic and electrical fields leads to orthogonal maps of the magnetic field and electrical potential on the scalp surface. This orthogonality means that an orthogonal localization direction is the best localization direction for both modalities (Malmivuo et al., 1997; Cohen and Halgren, 2003). These complementary features of the EEG and MEG signals are what make them good candidates for integration (Dale and Sereno, 1993; Baillet et al., 1999). The conjoint E/MEG analysis has improved the fidelity of EMSI localization, but has not entirely solved the problem of source localization ambiguity. It is the reduction of this remaining ambiguity where information from other brain imaging modalities may play a valuable role.

It is worth noting another purely technical advantage of MEG over EEG: MEG provides a reference-free recording of the actual magnetic field. Whenever EEG sensors capture scalp potentials, a reference electrode must be used as a ground to derive the signal of interest. A reference signal chosen in such a way can be arbitrarily biased relative to the EEG signal observed even when no neuronal sources are active. The unknown in an MEG signal obtained using SQUID sensors, is just a constant in time offset—the DC baseline. This baseline depends on the nearest flux quantum for which the flux-locked loop acquired lock (Vrba and Robinson, 2001, pg. 265). Although the choice of a reference value in EEG and the DC line in MEG do not influence the analysis of potential/field topographic maps, they do impact inverse solution algorithms which assume zero net source in the head, *i.e.* zero baseline. In general, the simple average reference across the electrodes is used and it has been shown to be a good approximation to the true reference signal (Michel et al., 2004, sec. 2.2).

Even if the reference value (baseline) is chosen correctly, both conventional EEG and MEG face obstacles in measuring the slowly changing DC component of the signal in the low frequency range ($f < 0.1\,\mathrm{Hz}$). In the case of EEG the problem is due to the often used coupling of the electrodes via capacitors, so that any DC component (slowly changing bias) of the EEG signal is filtered out. That leaves the researcher with non-zero frequency components of the signal, which often correspond to the most informative part of the signal as in the case of conventional ERP or frequency domain analysis. The DC-EEG component can be registered by using sensors with direct coupling and special scalp electrodes that are gel filled to eliminate changes of electrical impedance at the electrode-skin interface which can cause low frequency noise in the EEG signal. Although the MEG system does not require direct contact between sensors and skin, it is nevertheless subject to $1/f$ sensor noise which interferes with the measurement of the neuronal DC fields. In the last decade DC-MEG has been methodically refined by employing controlled brain-to-sensor modulation allowing the monitoring of low-frequency magnetic fields. Formalized DC-E/MEG techniques make it possible to perform E/MEG studies, which rely on the shift of DC and low frequency components of the signal; components that occur, for example, during epileptic seizures, hyperventilation, changes in vigilance states, cognitive or motor tasks.

### 8.2.2 Forward Modeling

The analysis of E/MEG signals often relies on the solution of two related problems. The *forward problem* concerns the calculation of scalp potentials (EEG) or magnetic fields near the scalp (MEG) given the neuronal currents in the brain, whereas the *inverse problem* involves estimating neuronal currents from the observed E/MEG data. The difficulty of solving the forward problem is reflected in the diversity of approaches that have been tried (see Mosher et al. (1999) for an overview and unified analysis of different methods).

The basic question posed by both the inverse and forward problems is how to model any neuronal activation so that the source of the electromagnetic field can be mapped onto the observed E/MEG signal. Assuming that localized and synchronized primary currents are the generators of the observed E/MEG signals, the most successful approach is to model the $i$-th source with a simple Equivalent Current Dipole (ECD) $\mathbf{q}_i$ (Brazier, 1949), uniquely defined by three factors: location represented by the vector $\mathbf{r}_i$, strength $q_i$, and orientation coefficients $\theta_i$. The orientation coefficient is defined by projections of the vector $\mathbf{q}_i$ into $L$ orthogonal Cartesian axes: $\theta_i = \mathbf{q}_i/q_i$. However, the orientation coefficient may be expressed by projections in two axes in the case of a MEG spherical model where the silent radial to the skull component has been removed, or even, just in a single axis if normality to the cortical surface is assumed. The ECD model made it possible to derive a tractable physical model linking neuronal activation and observed E/MEG signals. In case of $K$ simultaneously active sources at time $t$ the observed E/MEG signal at the sensor $\mathbf{x}_j$ positioned at $\mathbf{p}_j$ can be modeled as

$$\hat{\mathbf{x}}_j(\mathbf{r}_i, \mathbf{q}_i, t) = \sum_{i}^{K} \mathcal{G}(\mathbf{r}_i(t), \mathbf{p}_j) \cdot \mathbf{q}_i(t) + \epsilon, \tag{8.1}$$

where $\mathcal{G}$ is a *lead field* function which relates the $i$-th dipole and the potential (EEG) or magnetic field (MEG) observed at the $j$-th sensor; and $\epsilon$ is the sensor noise. In the given formulation, function $\mathcal{G}(\mathbf{r}_i(t), \mathbf{p}_j)$ returns a vector, where each element corresponds to the lead coefficient at the location $\mathbf{p}_j$ generated by a unit-strength dipole at position $\mathbf{r}_i(t)$ with the same orientation as the corresponding projection axis of $\theta_i$. The inner-product between the returned vector and dipole strength projections on the same coordinate axes yields a $j$-th sensor the measurement generated by the $i$-th dipole.

The forward model (8.1) can be solved at substantial computational expense using available numerical methods (Pruis et al., 1993) in combination with realistic structural information obtained from the MRI data (see Section 8.4.1). This high computational cost is acceptable when the forward model has to be computed once per subject and for a fixed number of dipole locations, but it can be prohibitive for dipole fitting, which requires a recomputation of the forward model for each step of non-linear optimization. For this reason, rough approximations of the head geometry and structure are often used: *e.g.* best-fit single sphere model which has a direct analytical solution (Zhang, 1995) or the multiple spheres model to accommodate for the difference in conductivity parameters across different tissues. Recently proposed MEG forward modeling methods for realistic isotropic volume conductors (Nolte, 2003, 2004) seem to be more accurate and faster than BEM, and hence may be useful substitutes for both crude analytical methods and computationally intensive finite-element numeric approximations. Generally, the solution of the forward problem is crucial for performing source localization using E/MEG, which is the main topic of the next section.

### 8.2.3 The Inverse Problem

#### Equivalent Current Dipole Models

The E/MEG inverse problem is very challenging (see Hämäläinen et al. (1993); Baillet et al. (2001a) for an overview of methods.) First, it relies on the solution of the forward problem, which can be computationally

expensive, especially in the case of realistic head modeling. Second, the lead-field function $\mathcal{G}$ from (8.1) is non-linear in $\mathbf{r}_i$, so that the forward model depends non-linearly on the locations of activations. It is because of this nonlinearity that the inverse problem is generally treated by non-linear optimization methods, which can lead to solutions being trapped in local minima. In case of Gaussian sensor noise, the best estimator for the reconstruction quality of the signal is the squared error between the obtained and modeled E/MEG data:

$$\mathcal{E}(\mathbf{r},\mathbf{q}) = \sum_{i}^{K}\sum_{t=t_1}^{t_2}\sum_{j}^{M}\big(\mathbf{x}_j(t) - \hat{\mathbf{x}}_j(\mathbf{r}_i,\mathbf{q}_i,t)\big)^2 + \lambda f(\mathbf{r},\mathbf{q}), \tag{8.2}$$

where $f(\mathbf{r},\mathbf{q}) > 0$ is often introduced to regularize the solution, *i.e.* to obtain the desired features of the estimated signal (*e.g.* smoothness in time, or in space, lowest energy or dispersion), and $\lambda > 0$ is used to vary the trade-off between the goodness of fit and the regularization term.

This least-squares model can be applied to the individual time-points ($t_1 = t_2$) ("moving dipole" model) or to a block ($t_1 < t_2$) of data points. If the sources are assumed not to change during the block ($t_1$,$t_2$), then the solution with time constant $\mathbf{q}_i(t) = \mathbf{q}_i$ is the target.

Other features derived from the data besides pure E/MEG signals as the argument $\mathbf{x}$ of (8.1) and (8.2) are often used: *e.g.* ERP/ERF waveforms which represent averaged E/MEG signals across multiple trials, mean map in the case of stable potential/field topography during some period of time, or signal frequency components to localize the sources of the oscillations of interest.

Depending on the treatment of (8.2), the inverse problem can be presented in a couple of different ways. The brute-force minimization of (8.2) in respect to both parameters $\mathbf{r}$ and $\mathbf{q}$, and the consideration of different $K$ neuronal sources, is generally called *ECD fitting*. Because of non-linear optimization, this approach works only for cases where there is a relatively small number of sources $K$, and therefore the inverse problem formulation is over-determined, *i.e.* (8.1) cannot be solved exactly ($\mathcal{E}(\mathbf{r},\mathbf{q}) > 0$). If fixed time locations of the target dipoles can be assumed, the search space of non-linear optimization is reduced and the optimization can be split into two steps: (a) non-linear optimization to find locations of the dipoles, and then (b) analysis to determine the strength of the dipoles. This assumption constitutes the so-called *spatiotemporal ECD model*.

Two other frameworks have been suggested as means of avoiding the pitfalls associated with non-linear optimization: Distributed ECD (DECD) and beamforming. We discuss these two approaches in detail in the next sections.

### Linear Inverse Methods: Distributed ECD

In case of multiple simultaneously active sources, an alternative to solving the inverse problem by ECD fitting is a distributed source model. We will use the label Distributed ECD (DECD) to refer to this type of model. The DECD is based on a spatial sampling of the brain volume and distributing the dipoles across all plausible and spatially small areas, which could be a source of neuronal activation. In such cases, fixed locations ($\mathbf{r}_i$) are available for each source/dipole, removing the necessity of non-linear optimization as in the case of the ECD fitting. The forward model (8.1) can be presented for a noiseless case in the matrix form

$$\mathbf{X} = \mathbf{G}\mathbf{Q}, \tag{8.3}$$

where $\mathbf{G}$, $M \times LN$ *lead field* matrix, is assumed to be static in time. The $j,i$-th entry of $\mathbf{G}$ describes how much a sensor $j$ is influenced by a dipole $i$, where $j$ varies over all sensors while $i$ varies over every possible source, or to be more specific, every axis-aligned component of every possible source: $g_{j\bar{\imath}} = \mathcal{G}(\mathbf{r}_i,\mathbf{p}_j)$. The vector $\bar{\imath}$ contains indices of $L$ such projections, *i.e.* $\bar{\imath} = [3i, 3i+1, 3i+2]$ when $L = 3$, and $\bar{\imath} = i$ when the dipole has a fixed known orientation. Using this notation, $\mathbf{G}_{\bar{\imath}}$ corresponds to the lead matrix for a single dipole $\mathbf{q}_i$. The $M \times T$ matrix $\mathbf{X}$

holds the E/MEG data, while the $LN \times T$ matrix $\mathbf{Q}$ (note that $\mathbf{Q}_{\bar{\imath}t} = \mathbf{q}_i(t)$) corresponds to the projections of the ECD's moment onto $L$ orthogonal axes.

The solution of (8.3) relies on finding an inverse $\mathbf{G}^+$ of the matrix $\mathbf{G}$ to express the estimate $\hat{\mathbf{Q}}$ in terms of $\mathbf{X}$

$$\hat{\mathbf{Q}} = \mathbf{G}^+\mathbf{X}, \tag{8.4}$$

and will produce a linear map $\mathbf{X} \longmapsto \hat{\mathbf{Q}}$. Other than being computationally convenient, there is not much reason to take this approach. The task is to minimize the error function (8.2), which can be generalized by the weighting of the data to account for the sensor noise and its covariance structure:

$$L(\mathbf{Q}) = \mathrm{tr}\big((\mathbf{X} - \mathbf{G}\mathbf{Q})^\top \mathbf{W}_\mathbf{X}^{-1}(\mathbf{X} - \mathbf{G}\mathbf{Q})\big), \tag{8.5}$$

where $\mathbf{W}_\mathbf{X}^{-1}$ is a weighting matrix in sensor space.

A zero-mean Gaussian signal can be characterized by the single covariance matrix $\mathbf{C}_\epsilon$. In case of a non-singular $\mathbf{C}_\epsilon$ we can use the most simple weighting scheme $\mathbf{W}_\mathbf{X} = \mathbf{C}_\epsilon$ to account for non-uniform and possibly correlated sensor noise.

Such a brute-force approach solves some problems of ECD modeling, specifically the requirement for a non-linear optimization, but, unfortunately, it introduces another problem: the linear system (8.3) is ill-posed and under-determined because the number of sampled possible source locations is much higher than the dimensionality of the input data space (which cannot exceed the number of sensors), *i.e.* $N \gg M$. Thus, there is an infinite number of solutions for the linear system because any combination of terms from the null space of $\mathbf{G}$ will satisfy equation (8.4) and fit the sensor noise perfectly. In other words, many different arrangements of the sources of neural activation within the brain can produce any given MEG or EEG map. To overcome such ambiguity, a regularization term is introduced into the error measure

$$L_r(\mathbf{Q}) = L(\mathbf{Q}) + \lambda f(\mathbf{Q}), \tag{8.6}$$

where $\lambda \geq 0$ controls the trade-off between the goodness of fit and the regularization term $f(\mathbf{Q})$.

The equation (8.6) can have different interpretations depending on the approach used to derive it and the meaning given to the regularization term $f(\mathbf{Q})$. All of the following methods provide the same result under specific conditions (Baillet et al., 2001a; Hauk, 2004): Bayesian methodology to maximize the posterior $p(\mathbf{Q}|\mathbf{X})$ assuming Gaussian prior on $\mathbf{Q}$ (Baillet and Garnero, 1997), Wiener estimator with proper $\mathbf{C}_\epsilon$ and $\mathbf{C}_S$, Tikhonov regularization to trade-off the goodness of fit (8.5) and the regularization term $f(\mathbf{Q}) = \mathrm{tr}(\mathbf{Q}^\top \mathbf{W}_\mathbf{Q}^{-1}\mathbf{Q})$ which attempts to find the solution with weighted by $\mathbf{W}_\mathbf{Q}^{-1}$ minimal 2nd norm. All the frameworks lead to the solution of the next general form

$$\mathbf{G}^+ = (\mathbf{G}^\top \mathbf{W}_\mathbf{X}^{-1}\mathbf{G} + \lambda \mathbf{W}_\mathbf{Q}^{-1})^{-1}\mathbf{G}^\top \mathbf{W}_\mathbf{X}^{-1}. \tag{8.7}$$

If and only if $\mathbf{W}_\mathbf{Q}$ and $\mathbf{W}_\mathbf{X}$ are positive definite (Grave de Peralta Menendez et al., 2004) (8.7) is equivalent to

$$\mathbf{G}^+ = \mathbf{W}_\mathbf{Q}\mathbf{G}^\top(\mathbf{G}\mathbf{W}_\mathbf{Q}\mathbf{G}^\top + \lambda \mathbf{W}_\mathbf{X})^{-1}. \tag{8.8}$$

In case when viable prior information about the source distribution is available $\mathbf{Q}_p$, it is easy to account for it by minimizing the deviation of the solution not from $\mathbf{0}$ (which constitutes the minimal 2nd norm solution $\mathbf{G}^+$), but from the prior $\mathbf{Q}_p$, *i.e.* $f(\mathbf{Q}) = \mathrm{tr}\big((\mathbf{Q} - \mathbf{Q}_p)^\top \mathbf{W}_\mathbf{Q}^{-1}(\mathbf{Q} - \mathbf{Q}_p)\big)$. Then (8.6) will be minimized at

$$\hat{\mathbf{Q}} = \mathbf{G}^+\mathbf{X} + (\mathbf{I} - \mathbf{G}^+\mathbf{G})\mathbf{Q}_p = \mathbf{Q}_p + \mathbf{G}^+(\mathbf{X} - \mathbf{G}\mathbf{Q}_p). \tag{8.9}$$

For the noiseless case, with a weighted $L_2$-norm regularizer, the Moore-Penrose pseudo-inverse gives the inverse $\mathbf{G}^+ = \mathbf{G}^\dagger$ by avoiding the null space projections of $\mathbf{G}$ in the solution, thus providing a unique solution with a minimal second norm $\mathbf{G}^\dagger = \mathbf{W}_\mathbf{Q}\mathbf{G}^\top(\mathbf{G}\mathbf{W}_\mathbf{Q}\mathbf{G}^\top)^{-1}$.

Taking $\mathbf{W_Q} = \mathbf{I}_N, \mathbf{W_X} = \mathbf{I}_M$ and $\mathbf{Q}_p = \mathbf{0}$ constitutes the simplest regularized minimum norm solution (Tikhonov regularization). Classically, $\lambda$ is found using cross-validation (Golub et al., 1979) or L-curve (Hansen, 1992) techniques, to decide how much of the noise power should be brought into the solution. Phillips et al. (2002b) suggested iterative method ReML where the conditional expectation of the source distribution and the regularization parameters are estimated jointly. Additional constraints can be added to impose an additional regularization: for instance temporal smoothness (Brooks et al., 1999).

As presented in (8.8), $\mathbf{G}^+$ can account for different features of the source or data space by incorporating them correspondingly into $\mathbf{W_Q}$ and $\mathbf{W_X}$. Next data-driven features are commonly used in EMSI

- $\mathbf{W_X} = \mathbf{C}_\epsilon$ accounts for any possible noise covariance structure or, if $\mathbf{C}_\epsilon$ is diagonal, will scale the error terms according to the noise level of each sensor;
- $\mathbf{W_Q} = \mathbf{W}_{\mathbf{C}_S} = \mathbf{C}_S$ accounts for prior knowledge of the sources covariance structure.

$\mathbf{W_Q}$ can also account for different spatial features

- $\mathbf{W_Q} = \mathbf{W}_{\text{n}} = \left(\text{diag}\left(\mathbf{G}^\top\mathbf{G}\right)\right)^{-1}$ normalizes the columns of the matrix $\mathbf{G}$ to account for deep sources by penalizing voxels too close to the sensors (Lawson and Hanson, 1974; Jeffs et al., 1987);
- $\mathbf{W_Q} = \mathbf{W}_{\text{gm}}$, where the $i$-th diagonal element incorporates the gray matter content in the area of the $i$-th dipole (Phillips et al., 2002a), *i.e.* the probability of having a large population of neurons capable of creating the detected E/MEG signal;
- $\mathbf{W_Q} = (\mathbf{W}_a{}^\top\mathbf{W}_a)^{-1}$, where rows of $\mathbf{W}_a$ represent averaging coefficients for each source (Backus and Gilbert, 1968). So far only geometrical (Grave de Peralta Menendez and Gonzalez Andino, 1998) or biophysical averaging matrices (Grave de Peralta Menendez et al., 2004) were suggested;
- $\mathbf{W_Q}$ incorporates the first-order spatial derivative of the image (Wang et al., 1992) or Laplacian form (Pascual-Marqui et al., 1994).

Features defined by the diagonal matrices (*e.g.* $\mathbf{W}_{\text{n}}$ and $\mathbf{W}_{\text{gm}}$) can be combined through the simple matrix product. An alternative approach is to present $\mathbf{W_Q}$ in terms of a linear basis set of the individual $\mathbf{W_Q}$ factors, *i.e.* $\mathbf{W_Q} = \mu_1\mathbf{W}_{\text{n}} + \mu_2\mathbf{W}_{\text{gm}} + \cdots$, with later optimization of $\mu_i$ via the EM algorithm (Phillips et al., 2002a).

To better condition the under-determined linear inverse problem (8.4), Phillips et al. (2002a) suggested to perform the inverse operation (8.4) in the space of the largest eigenvectors of the $\mathbf{W_Q}$. Such preprocessing can also be done in the temporal domain, when a similar sub-space selection is performed using prior temporal covariance matrix, thus effectively selecting the frequency power spectrum of the estimated sources.

Careful selection of the described features of data and source spaces helps to improve the fidelity of the DECD solution. Nevertheless, the inherent ambiguity of the inverse solution precludes achieving a high degree of localization precision. It is for this reason that additional spatial information about the source space, readily available from other functional modalities such as fMRI and PET, can help to condition the DECD solution (Section 8.4.3).

### Beamforming

Beamforming (sometimes called a spatial filter or a virtual sensor) is another way to solve the inverse problem, which actually does not directly minimize (8.2). A beamformer attempts to find a linear combination of the input data $\hat{\mathbf{q}}_i = \mathbf{F}^i\mathbf{x}$, which represents the neuronal activity of each dipole $\mathbf{q}_i$ in the best possible way one at a given time. As in DECD methods, the search space is sampled, but, in contrast to the DECD approach, the beamformer does not try to fit all the observed data at once.

The linearly constrained minimum variance (LCMV) beamformer (Van Veen et al., 1997) looks for a spatial filter defined as $\mathbf{F}^i$ of size $M \times L$ minimizing the output energy ${\mathbf{F}^i}^\top \mathbf{C}_X \mathbf{F}^i$ under the constraint that only $\mathbf{q}_i$ is active at that time, *i.e.* that there is no attenuation of the signal of interest: $\mathbf{F}^k \mathbf{G}_{\bar{\imath}} = \delta_{ki} \mathbf{I}_L$, where the Kronecker delta $\delta_{ki} = 1$ only if $k = i$ and 0 otherwise. Because the beamforming filter $\mathbf{F}^i$ for the $i$-th dipole is defined independently from the other possible dipoles, index $i$ will be dropped from the derived results for the clarity of presentation.

The constrained minimization, solved using Lagrange multipliers, yields

$$\mathbf{F} = ({\mathbf{G}_{\bar{\imath}}}^\top \mathbf{C}_X^{-1} \mathbf{G}_{\bar{\imath}})^{-1} {\mathbf{G}_{\bar{\imath}}}^\top \mathbf{C}_X^{-1} \tag{8.10}$$

This solution is equivalent to (8.7), when applied to a single dipole with the regularization term omitted. Source localization is performed using (8.10) to compute the variance of every dipole $\mathbf{q}$, which, in the case of uncorrelated dipole moments, is

$$\nu_{\mathbf{q}} = \mathrm{tr}\big(({\mathbf{G}_{\bar{\imath}}}^\top \mathbf{C}_X^{-1} \mathbf{G}_{\bar{\imath}})^{-1}\big). \tag{8.11}$$

The noise-sensitivity of (8.11) can be reduced by using the noise variance of each dipole as normalizing factor $\nu_\epsilon = \mathrm{tr}\big(({\mathbf{G}_{\bar{\imath}}}^\top \mathbf{C}_\epsilon^{-1} \mathbf{G}_{\bar{\imath}})^{-1}\big)$. This produces the so-called *neural activity index*

$$z = \frac{\nu_{\mathbf{q}}}{\nu_\epsilon}. \tag{8.12}$$

An alternative beamformer, *synthetic aperture magnetometry* or SAM (Robinson and Vrba, 1999), is similar to the LCMV if the orientation of the dipole is defined, but it is quite different in the case of a dipole with an arbitrary orientation. We define a vector of lead coefficients $\mathbf{g}_i(\theta)$ as a function of the dipole orientation. This returns a single vector for the orientation $\theta$ of the $i$-th dipole, as opposed to the earlier formulation in which the $L$ columns of $\mathbf{G}_{\bar{\imath}}$ played a similar role. With this new formulation, we construct the spatial filter

$$\mathbf{f}(\theta) = \frac{1}{\mathbf{g}_i(\theta)^\top \mathbf{C}_X^{-1} \mathbf{g}_i(\theta)} \mathbf{g}_i(\theta)^\top (\mathbf{C}_X + \lambda \mathbf{C}_\epsilon)^{-1} \tag{8.13}$$

which, under standard assumptions, is an optimal linear estimator of the time course of the $i$-th dipole. The variance of the dipole, accordingly, is also a function of $\theta$, specifically $\nu_{\mathbf{q}}(\theta) = 1/\big(\mathbf{g}_i(\theta)^\top \mathbf{C}_X^{-1} \mathbf{g}_i(\theta)\big)$. To compute the neuronal activity index the original SAM formulation uses a slightly different normalization factor $\nu_\epsilon(\theta) = \mathbf{f}(\theta)^\top \mathbf{C}_\epsilon \mathbf{f}(\theta)$, which yields a different result if the noise variance in $\mathbf{C}_\epsilon$ is not equal across the sensors.

The unknown value of $\theta$ is found via a non-linear optimization of the neuronal activity index for the dipole:

$$\theta = \arg\max_\vartheta \frac{\nu_{\mathbf{q}}(\vartheta)}{\nu_\epsilon(\vartheta)}.$$

Despite the pitfalls of non-linear optimization, SAM filtering provides a higher SNR to LCMV by bringing less than half of the noise power into the solution. In addition, SAM filtering results in sharper peaks of the distribution of neuronal activity index over the volume (Vrba and Robinson, 2000).

Having computed $\nu_{\mathbf{q}}$ and $\nu_\epsilon$ using SAM or LCMV for the two experimental conditions: passive ($p$) and active ($a$), it is possible to compute a pseudo-$t$ value $\hat{t}$ for each location across the two conditions

$$\hat{t} = \frac{\nu_{\mathbf{q}}^{(a)} - \nu_{\mathbf{q}}^{(p)}}{\nu_\epsilon^{(a)} + \nu_\epsilon^{(p)}}. \tag{8.14}$$

Such an approach provides the possibility of considering experimental design in the analysis of E/MEG localization.

Unlike ECD, beamforming does not require prior knowledge of the number of sources, nor does it search for a solution in an underdetermined linear system as does DECD. For these reasons, beamforming remains the favorite method of many researchers in EMSI and has been suggested for use in the integrative analysis of E/MEG and fMRI which we cover in Section 8.4.3.

## 8.3 Multimodal Experiments

Obtaining non-corrupted simultaneous recordings of EEG and fMRI is a difficult task due to interference between the strong MR field and the EEG acquisition system. Because of this limitation, a concurrent EEG/fMRI experiment requires specialized design and preprocessing techniques to prepare the data for the analysis. The instrumental approaches described in this section are specific to collecting concurrent EEG and fMRI data. For obvious reasons MEG and fMRI data must be acquired separately in two sessions. However, even when MR and MEG are used sequentially, there is the possibility of contamination from the magnetization of a subject's metallic implants which can potentially disturb MEG acquisition if it is performed shortly after the MR experiment.

### 8.3.1 Measuring EEG During MRI: Challenges and Approaches

Developing methods for the integrative analysis of EEG and fMRI data is difficult for several reasons, not the least of which is the concurrent acquisition of EEG and fMRI itself has proved challenging. The nature of the problem is expressed by Faraday's law of induction: a time varying magnetic field in a wire loop induces an electromotive force (EMF) proportional in strength to the area of the wire loop and to the rate of change of the magnetic field component orthogonal to the area. When EEG electrodes are placed in a strong ambient magnetic field resulting in the EMF effect several undesirable complications arise:

- Rapidly changing MR gradient fields and RF pulses may induce voltages in the EEG leads placed inside the MR scanner. Introduced potentials may greatly obscure the EEG signal (Ives et al., 1993). This kind of artifact is a real concern for concurrent EEG/MRI acquisition. Due to the deterministic nature of MR interference, hardware and algorithmic solutions may be able to unmask the EEG signal from MR disturbances. For example, Allen et al. (2000) suggested an average waveform subtraction method to remove MR artifacts which seems to be effective (Salek-Haddadi et al., 2002). However, it is important to note that time variations of the MR artifact waveform can reduce the success of this method (Cohen et al., 2001; Cohen, 2004). The problem can be resolved through hardware modification that increases the precision of the synchronization of MR and EEG systems (Anami et al., 2003) or during post-processing by using precise timings of the MR pulses during EEG waveform averaging (Cohen et al., 2001). Other techniques that have been proposed to reduce MR and ballistocardiographic artifacts include spectral domain filtering, spatial Laplacian filtering, PCA (Fig. 8.1), and ICA (see Sijbers et al., 1999; Bonmassar et al., 2002; Garreffa et al., 2003; Negishi et al., 2004; Srivastava et al., 2005)

- Even a slight motion of the EEG electrodes within the strong static field of the magnet can induce significant EMF (Hill et al., 1995; Kruggel et al., 2000). For instance, native pulsatile motion related to a heart beat yields a ballistocardiographic artifact in the EEG that can be roughly the same magnitude as the EEG signals themselves (Ives et al., 1993; Goldman et al., 2000). Usually such artifacts are removed by the same average waveform subtraction method, where the waveform is an averaged response to each heartbeat.

- Induced electric currents can heat up the electrode leads to painful or even potentially dangerous levels, such as to the point of burning the subject (Lemieux et al., 1997). Current-limiting electric components (resistors, JFET transistors, *etc.*) are usually necessary to prevent the development of nuisance currents which can have direct contact with subject's scalp. Simulations show the safe power range that should be used for some coil/power/sensors configuration to comply with FDA guidelines (Angelone et al., 2004).

Another concern is the impact of EEG electrodes on the quality of MR images. The introduction of EEG equipment into the scanner can potentially disturb the homogeneity of the magnetic field and distort the resulting MR images (Ives et al., 1993; Lazeyras et al., 2001). Recent investigations show that such artifacts can be

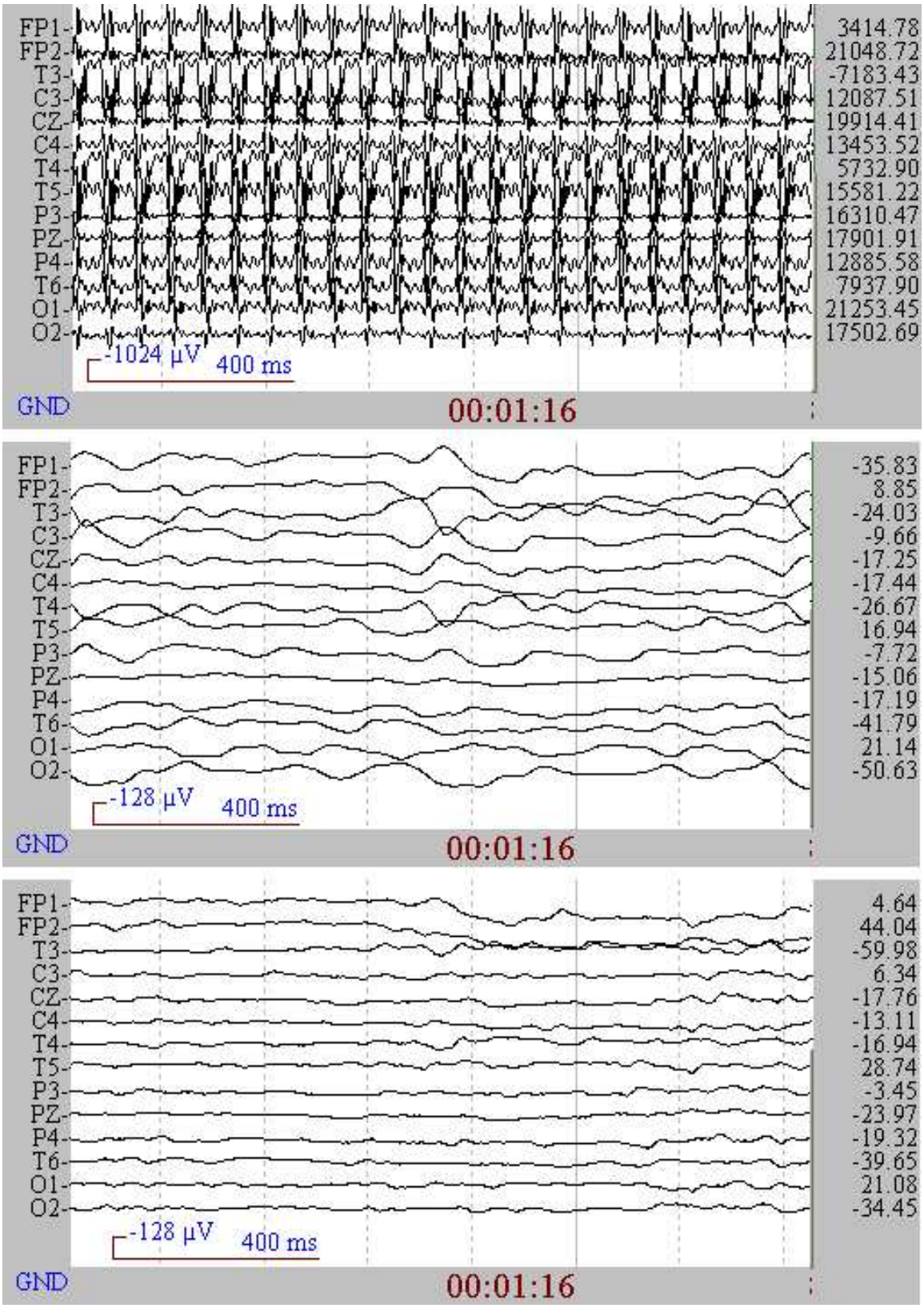


Figure 8.1: EEG MR artifact removal using PCA. EEG taken inside the magnet (top); EEG after PCA-based artifact removal but with ballistocardiographic artifacts present (center); EEG with all artifacts removed (bottom). After artifact removal it can be seen that the subject closed his eyes at time 75.9 s. (Courtesy of M. Negishi and colleagues, Yale University School of Medicine.)

effectively avoided (Krakow et al., 2000) by using specially designed EEG equipment (Goldman et al., 2000): specialized geometries, and new "MR-safe" materials (carbon fiber, plastic) for the leads. To test the influence of a given EEG system on fMRI data, a comparison of the data collected both with and without the EEG system being present, should be conducted. Analysis of such data usually demonstrates the same activation patterns in two conditions (Lazeyras et al., 2001), although a general decrease in fMRI SNR is observed when EEG is present in the magnet. A correction to the brain matter conductivities (which are used for forward E/MEG modeling) for the Hall effect finds the following first-order correction to be negligible: $\sigma_H = 4.1 \times 10^{-8}\sigma$ for $B = 1.5\,\mathrm{T}$ Bonmassar et al. (2001).

### 8.3.2 Experimental Design Limitations

There are two ways of avoiding the difficulties associated with collecting EEG data in the magnet: (1) collect EEG and MRI data separately, or (2) use an experimental paradigm that can work around the potential contamination between the two modalities. The decision between these two alternatives will depend on the constraints associated with research goals and methodology. For example, if an experiment can be repeated more than once with a high degree of reliability of the data, separate E/MEG and fMRI acquisition may be appropriate (Menon et al., 1997; Horovitz et al., 2002, 2004; Schulz et al., 2004). In cases when simultaneous measurements are essential for the experimental objective (e.g., cognitive experiments where a subject's state might influence the results as in monitoring of spontaneous activity or sleep state changes), one of the following protocols can be chosen:

**Triggered fMRI:** detected EEG activity of interest (epileptic discharge, *etc.*) triggers MRI acquisition (Warach et al., 1996; Seeck et al., 1998; Lazeyras et al., 2000; Krakow et al., 2001). Due to the slowness of the HR, relevant changes in the BOLD signal can be registered 4–8 s after the event. The EEG signal can settle quickly after the end of the previous MRI block (Goldman et al., 2000), so it is acquired without artifacts caused by RF pulses or gradient fields that are present only during the MRI acquisition block. Note that ballistocardiographic and motion-caused artifacts still can be present and will require post-processing in order to be eliminated. Although this is an elegant solution and has been used with some success in the localization of epileptic seizures, this protocol does have drawbacks. Specifically, it imposes a limitation on the amount of subsequent EEG activity that can be monitored if the EEG high-pass filters do not settle down soon after the MR sequence is terminated (Huang-Hellinger et al., 1995). In this case, EEG hardware that does not have a long relaxation period must be used. Another drawback with this approach is that it requires online EEG signal monitoring to trigger the fMRI acquisition in case of spontaneous activity. Often experiments of this kind are called *EEG-correlated fMRI* due to the fact that offline fMRI data time analysis implicitly uses EEG triggers as the event onsets (Salek-Haddadi et al., 2002);

**Interleaved EEG/fMRI:** the experiment protocol consists of time blocks and only a single modality is acquired during each time-block (Bonmassar et al., 2001; Makiranta et al., 2004). This means that every stimulus has to be presented at least once per modality. To analyze ERP and fMRI activations, the triggered fMRI protocol can be used with every stimulus presentation so that EEG and MR are sequentially acquired in order to capture a clean E/MEG signal followed by the delayed HR (Sommer et al., 2003);

**Simultaneous fMRI/EEG:** pre-processing of the EEG signal mentioned in Section 8.3.1 is used to remove the MR-caused artifacts and to obtain an estimate of the true EEG signal. However, neither of the existing artifact removing methods is proved to be general enough to work for every type of EEG experiment and analysis. It is especially difficult to use such an acquisition scheme for cognitive experiments in which the EEG evoked responses of interest can be of small amplitude and completely overwhelmed by the MR noise (Schomer et al., 2000).

## 8.4 Multimodal Analysis

There is an increasing number of reported E/MEG/fMRI conjoint studies, which attempt to gain the advantages of a multimodal analysis for experiments involving perceptual and cognitive processes: visual perception (Lazeyras et al., 2001; Singh et al., 2002; Sommer et al., 2003; Vanni et al., 2004) and motor activation (Lazeyras et al., 2001), somatosensory mapping (Korvenoja et al., 1999; Schulz et al., 2004), fMRI correlates of EEG rhythms (Cohen et al., 2001; Goldman et al., 2002; Moosmann et al., 2003; Laufs et al., 2003a; Makiranta et al., 2004), arousal and attention interaction (Foucher et al., 2004), auditory oddball tasks (Horovitz et al., 2002), passive frequency oddball (Liebenthal et al., 2003), illusory figures in visual oddball tasks (Kruggel et al., 2001), target detection (Menon et al., 1997; Mulert et al., 2004), face perception (Horovitz et al., 2004), sleep (Huang-Hellinger et al., 1995), language tasks (Vitacco et al., 2002; Singh et al., 2002), and epilepsy (Warach et al., 1996; Seeck et al., 1998; Krakow et al., 1999a,b, 2001; Lantz et al., 2001; Lemieux et al., 2001; Waites et al., 2005).

This section starts with an explanation of the role of anatomical MRI in multimodal experiments followed by a description of multimodal analysis methods used in the above mentioned studies or test-driven on the simulated data.

### 8.4.1 Using Anatomical MRI

The difference in captured MRI contrasts (proton densities (PD) or T1, T2 relaxation times) for different types of organic tissue makes possible the non-invasive collection of information about the structural organization of the brain. In addition, a regular gradient or spin echo EPI sequence is capable of detecting transient or subtle changes of the magnetic field in cortical tissue caused by neuronal activation (Bodurka and Bandettini, 2002; Xiong et al., 2003). However, direct application of MRI to capture functional activity remains limited due to a low signal-to-noise ratio (SNR) which is why MRI is often labelled *anatomical*. The next section briefly describes the analysis of acquired high-resolution 3D images of the brain and how obtained structural information can be used to analyze data collected from other modalities.

#### Registration of EEG and MEG to MRI

If an EEG experiment is performed inside the magnet, it is possible to "mark" (Lagerlund et al., 1993) the location of the EEG sensors to make them distinguishable on the anatomical MRI. Coordinates for these locations can then be found either manually or automatically (Sijbers et al., 2000) and will lie in MRI coordinate system. In case when MR and E/MEG data are acquired in separate sessions, spatial registration between E/MEG and MRI coordinate systems must be performed before any anatomical information can be introduced into the analysis of E/MEG data. There are two general possible ways for performing registration between MRI and E/MEG data: (a) registering a limited set of fiducial points or (b) aligning scalp surfaces obtained during MRI with a digitization of the scalp during E/MEG. Methods based on the alignment of the scalp surfaces (or points clouds) considered to perform better than those using fiducial-points (Schwartz et al., 1996; Huppertz et al., 1998; Kozinska et al., 2001; Lamm et al., 2001), but are more computationally demanding and rely on iterative optimization. In addition, it can be time consuming to obtain the dense digitization of the subject's head using a single point 3D digitizer. For these reasons the fiducial points approach remains the preferred E/MEG/MRI registration method (for instance Lagerlund et al., 1993; Towle et al., 1993). The fiducial points method involves the alignment of a limited set of points, which have a strict known correspondence between the two spaces, so that each fiducial point in E/MEG space with coordinates ($\mathbf{x}_i^E$) has a corresponding known point ($\mathbf{x}_i^M$) in MRI space. Such coupling removes the possibility of being trapped in the local minima of the iterative surface aligning methods and makes registration simple and fast. The precision of the derived transformation can be increased by adding more pairs

of corresponding E/MEG and MRI points. A more detailed description of the registration method using fiducial points follows.

Locations of the fiducial points (*e.g.* anatomical points: nasion, inion, pre-auricular points or tragus of the left and right earlobes, vertex; MRI-visible capsules or even bite-bar points (Singh et al., 1997; Adjamian et al., 2004)) are captured together with the locations of E/MEG sensors using a 3D digitizer and then matched to the locations of corresponding fiducial points obtained from the analysis of the MRI for the same subject. A 3D rigid transformation of the points from the E/MEG ($\mathbf{x}^E$) to the MRI coordinate system ($\mathbf{x}^{E\to M}$) can be defined by the rotation matrix $\mathbf{R}$ and translation vector $\mathbf{v}$, so that $\mathbf{x}^{E\to M} = \mathbf{R}\mathbf{x}_i^E + \mathbf{v}$. Commonly, the quadratic mis-registration error measure is the subject to minimization $\varepsilon(\mathbf{R},\mathbf{v}) = \sum_i^P (\mathbf{x}_i^M - \mathbf{x}^{E\to M})^2$, where $P$ is the number of the points. Solutions can be found with simplified geometrical formulations (Wieringa et al., 1993), or iterative search optimization using Powell's algorithm (Singh et al., 1997). Such simplifications or complications are not necessary because the analytical form solutions have been derived in other fields (Horn, 1987; Horn et al., 1988), and they are often used in the surface matching methods earlier discussed. For instance, quaternions (vectors in $L_4$) can be natively used to describe a rotation in 3D space leading to a straightforward solution of the registration problem[2] (Horn, 1987). This method is simple to implement. Its precision rapidly increases with the number of fiducial points, reaching the performance of surface matching algorithms cheaply and efficiently.

### Segmentation and Tessellation

PD or T1/T2 3D MR images can be used to segment different brain tissues (white matter, gray matter, cerebrospinal fluid (CSF), skull, scalp) as well as abnormal formations (tumors) (Dale and Sereno, 1993; Nielsen, 2001). Different kinds of MR contrasts are optimal for the segmentation of the different kinds of head and brain structures. For instance, PD-weighted MRI yields superior segmentation of the inner and outer skull surfaces because bones have much smaller water content than brain tissue, making the skull easily distinguishable on PD images. On the other hand, exploiting T1 and T2 relaxation time differences between various sorts of brain tissue leads to higher quality segmentation of structures within the brain.

Using triangulation (tessellation) and interpolation it is possible to create fine-grained smooth mesh representations or tetrahedral assemblies of the segmented tissues (Poupon, 1999; Dale et al., 1999; Shattuck and Leahy, 2002). Obtained 3D mesh of the cortical surface alone brings valuable information to the analysis of E/MEG

[2]To find the minimum of the error function $\varepsilon(\mathbf{R},\mathbf{v})$, we need merely to calculate a principal eigenvector

$$\mathbf{r} = \max\_\text{eigenvector} \begin{bmatrix} \operatorname{tr}(\mathbf{\Sigma}) & \mathbf{\Delta}^\top \\ \mathbf{\Delta} & \mathbf{\Sigma} + \mathbf{\Sigma}^\top - \operatorname{tr}(\mathbf{\Sigma})\mathbf{I}_3 \end{bmatrix} \tag{8.15}$$

where

$$\bar{\mathbf{x}} = \tfrac{1}{P}\sum_i^P \mathbf{x}_i \qquad \mathbf{\Sigma} = \tfrac{1}{P}\sum_i^P (\mathbf{x}_i^E - \bar{\mathbf{x}}^E)(\mathbf{x}_i^M - \bar{\mathbf{x}}^M)^\top \qquad \mathbf{\Delta} = \begin{bmatrix} (\mathbf{\Sigma} - \mathbf{\Sigma}^\top)_{23} \\ (\mathbf{\Sigma} - \mathbf{\Sigma}^\top)_{31} \\ (\mathbf{\Sigma} - \mathbf{\Sigma}^\top)_{12} \end{bmatrix}$$

The eigenvector $\mathbf{r}$ can be assumed to be normalized (unit length). Regarded as a quaternion, $\mathbf{r} = [r_0, r_1, r_2, r_3]^\top$ uniquely defines the rotation. This can be converted into a conventional rotation matrix

$$\mathbf{R} = \begin{bmatrix} r_0^2 + r_1^2 - r_2^2 - r_3^2 & 2(r_1 r_2 - r_0 r_3) & 2(r_1 r_3 + r_0 r_2) \\ 2(r_1 r_2 + r_0 r_3) & r_0^2 + r_2^2 - r_1^2 - r_3^2 & 2(r_2 r_3 - r_0 r_1) \\ 2(r_1 r_3 - r_0 r_2) & 2(r_2 r_3 + r_0 r_1) & r_0^2 + r_3^2 - r_1^2 - r_2^2 \end{bmatrix}.$$

The translation vector is then simply $\mathbf{v} = \bar{\mathbf{x}}^M - \mathbf{R}\bar{\mathbf{x}}^E$.

signals (Castellano, 1999): the physiology of the neuronal generators can be considered, allowing one to limit the search space for activated sources to the gray matter regions and oriented orthogonally or nearly so to the cortical surface (Nunez, 1981; Dale and Sereno, 1993).

Monte Carlo studies (Liu et al., 1998) tested the influence of the orientation constraint in the case of the DECD model and showed that such constraint leads to much better conditioning of the inverse problem while still being robust to the error of the assumed cortical surface: random deviation of the orientation in $30^\circ$ range leads to just a slight increase of distortion, thus not significantly affecting the accuracy of the localization procedure. Anatomical constraints improve the localization and contrast of beamforming imaging methods as well, but the use of anatomical constraints found to be advantageous only in case of good MRI/E/MEG coregistration (Hillebrand and Barnes, 2003).

#### Forward Modeling of EEG and MEG

Volumetric structures derived from the tessellation procedure are used to create a realistic geometry of the head, which is crucial for the forward modeling of E/MEG fields. Previously, rough approximations based on best-fit single/multiple sphere models were developed to overcome the burden of creating realistic head geometry, but they became less favorable as the increased availability of powerful computational resources made more realistic modeling possible. Spatial information is especially important for EEG forward modeling due to the fact that it is more strongly affected by the conductivities of the skull and the scalp than the MEG forward model. Such inhomogeneities might not affect the magnetic field at all in case of a spherical head model, when only the inner skull surface is of the main concern for the forward modeling.

There are four numerical methods available to solve the E/MEG modeling problem, and the Boundary Elements Method (BEM) (Hamalainen and Sarvas, 1989) is the most commonly used when isotropy (direction independence) of the matters is assumed, so that only boundary meshes obtained by the tessellation process are required. It was shown, however, that anisotropy of the skull (Marin et al., 1998) and white-matter (Wolters et al., 2001) can bias EEG and MEG forward models. To solve the forward problem in the case of an anisotropic medium, the head volume is presented by a large assembly of small homogeneous tetrahedrons, and a Finite Elements Method (FEM) (Miller and Henriquez, 1990) is used to approximate the solution. Another possible way is to use the Finite Difference Method (FDM) on a regular computational mesh (Saleheen and Ng, 1997). Table 8.2 lists some publicly available software which can help performing the forward E/MEG modeling. Forward modeling of E/MEG signal rely on the knowledge of matter conductivities. Common values of conductivities for different tissues can be found in the literature (Geddes and Baker, 1967), or can be estimated on a per-subject basis using Electrical Impedance Tomography (EIT) (Goncalves et al., 2003) or Diffusion Tensor (DT) (Tuch et al., 2001) MRI.

### 8.4.2 Forward Modeling of BOLD Signal

The successful analysis of the results of a multimodal experiment remains problematic. The main problem of multimodal analysis is the absence of a general unifying account of the BOLD fMRI signal in terms of the characteristics of a neuronal response. Various models have been suggested, on one hand they include naive modeling of BOLD signal in the context of a Linear Time Invariant System (LTIS). On the other hand there are general models of the BOLD signal in terms of detailed biophysical processes (*Balloon* (Buxton and Frank, 1997) or *Vein and Capillary* (Seiyama et al., 2004) models). The naive models are not general enough to explain the variability of the BOLD signal, whereas complex parametric models that rely heavily on a prior knowledge of nuisance parameters (due to biophysical details), and do not have a reliable and straightforward means of estimation. This fact makes it unlikely to use such comprehensive models as reliable generative models of the

BOLD signal. In the following section we describe modeling issues in greater detail to further underline the limited applicability of many multimodal analysis methods covered in Section 8.4.3.

### Convolutional Model of BOLD Signal

Various experimenters had originally focused on simple contrast designs such as block design paradigms in order to exploit the presumed linearity between their design parameters and the HR. This assumption depends critically on the ability of the block design to amplify the SNR and the implicit belief that the HR possess more temporal resolution than indicated by the TR.

In order to account for the present autocorrelation of the HR caused by its temporal dispersive nature, Friston et al. (1994) suggested to model HR with a LTIS. To describe the output of such a system, a convolution of an input (joint intrinsic and evoked neuronal activity $q(t)$) with a hemodynamic response function (HRF) $h(t)$ is used to model the HR

$$b(t) = (h * q)(t). \tag{8.16}$$

Localized neuronal activity itself is not readily available via means of non-invasive imaging, therefore it is more appropriate to verify LTIS modeling on real data as a function of parameters of the presented stimuli (*i.e.* duration, contrast).

The convolutional model was used on real data to demonstrate linearity between the BOLD response and the parameters of presented stimuli (Boynton et al., 1996; Cohen, 1997). In fact, many experimenters have shown apparent agreement between LTIS modeling and real data. Specificly it has been possible to model responses to longer stimuli durations by constructing them using the responses to shorter duration stimuli, which is consistent with LTIS modeling. Because of the predictive success, its relative simplicity of application and resulting ignorance of biophysical details this modeling approach became widely accepted. Unfortunately LTIS as a modeling constraint is very weak therefore allowing an arbitrary choice of parametric HRF based only on preference and familiarity.

Over the years multiple models for the HRF have been suggested. The most popular and widely used up until now is a single probability density function (PDF) of Gamma distribution by Lange and Zeger (1997). It was elaborated by Glover (1999) to perform the deconvolution of the HR signal, and the nuisance parameters $(n_1, t_1, n_2, t_2, a_2)$ of the next HRF were estimated for motor and auditory areas

$$h(t) = \frac{1}{c_1}\, t^{n_1}\, e^{-t/t_1} - \frac{a_2}{c_2}\, t^{n_2}\, e^{-t/t_2} \qquad \text{where} \qquad c_i = \max_t t^{n_i}\, e^{-t/t_i} = \left(\frac{e}{n_i t_i}\right)^{-n_i} \tag{8.17}$$

which can be described as the sum of two unscaled PDFs of Gamma distribution. The first term captures the positive BOLD HR and the second term is to capture the overshoot often observed in the BOLD signal. Many other simple and as well as more sophisticated models of HRF were suggested: Poisson PDF (Friston et al., 1994), Gaussians (Rajapakse et al., 1998), Bayesian derivations (Ciuciu et al., 2003; Gitelman et al., 2003; Marrelec et al., 2003) and others. The particular choice of any of them was primarily dictated by some other than biophysics motivation: easy Fourier transformation, presence of post-response dip or "best-fit" properties.

Since the suggestion of the convolutional model describing BOLD response, different aspects of HR linearity became an actively debated question. If HR is linear, then what features of the stimulus (*e.g.* duration, intensity) or neuronal activation (*e.g.* firing frequency, field potentials, frequency power) does it vary linearly with? As the first approximation, it is important to define the ranges of the above mentioned parameters in which HR was found to behave linearly. For example, early linearity tests (Glover, 1999) showed the difficulty in predicting long duration stimuli based on an estimated HR from shorter duration stimuli. Soltysik et al. (2004) reviewed existing papers describing different aspects of non-linearity in BOLD HR and attempted to determine the ranges of linearity in respect to stimuli duration in three cortical areas: motor, visual and auditory complex. The results

of these analyses have shown that although there is a strong non-linearity observed on small stimuli durations, long stimuli durations show higher degree of linearity.

It appears that a simple convolutional model generally is not capable of describing the BOLD responses in terms of the experimental design parameters if such are varying in a wide range during the experiment. Nevertheless LTIS might be more appropriate to model BOLD response in terms of neuronal activation if most of the non-linearity in the experimental design can be explained by the non-linearity of the neuronal activation itself.

**Neurophysiologic Constraints**

In the previous section we explored the subject of linearity between the experimental design parameters and the observed BOLD signal. For the purpose of this review it may be more interesting to explore the relation between neuronal activity and HR.

It is known that E/MEG signals are produced by large-scale synchronous neuronal activity, whereas the nature of the BOLD signal is not clearly understood. The BOLD signal does not seem to correspond to the neural activity that consumes the most energy (Attwell and Iadecola, 2002), as early researchers believed. Furthermore, the transformation between the electrophysiological indicators of neuronal activity and the BOLD signal cannot be linear for the entire dynamic range, under all experimental conditions and across all the brain areas. Generally, a transformation function cannot be linear since the BOLD signal is driven by a number of "nuisance" physiologic processes such as cerebral metabolic oxygen consumption ($CMRO_2$), cerebral blood flow (CBF) and cerebral blood volume (CBV) as suggested by the *Balloon model* (Buxton and Frank, 1997), which are not generally linear.

Due to the indirect nature of the BOLD signal as a tool to measure neuronal activity, in many multimodal experiments a preliminary comparative study is done first in order to assess the localization disagreement across different modalities. Spatial displacement is often found to be very consistent across multiple runs or experiments (see Section 8.4.3 for an example). Specifically, observed differences can potentially be caused by the variability in the cell types and neuronal activities producing each particular signal of interest Nunez and Silberstein (2000). That is why it is important first to discover the types of neuronal activations that are primary sources of the BOLD signal. Some progress on this issue has been made. A series of papers generated by a project to cast light on the relationship between the BOLD signal and neurophysiology, have argued that local field potentials (LFP) serve a primary role in predicting BOLD signal (Logothetis and Wandell, 2004, and references 27, 29, 54, 55 and 81 therein). This work countered the common belief that spiking activity was the source of the BOLD signal (for example Arthurs and Boniface, 2002) by demonstrating a closer relation of the observed visually evoked HR to the local field potentials (LFP) of neurons than to the spiking activity. This result places most of the reported non-linearity between experimental design and observed HR into the non-linearity of the neural response, which would benefit a multimodal analysis.

Note that the extracellular recordings experiments described above, were carried out over a small ROIs, therefore they inherit the parameters of underlying hemodynamic processes for the given limited area. Thus, even if LFP is taken as the primary electrophysiological indicator of the neuronal activity causing BOLD signal, the relationship between the neuronal activity and the hemodynamic processes on a larger scale remains an open question.

Since near-infrared optical imaging (NIOI) is capable of capturing the individual characteristics of cerebral hemodynamics such as total, oxy-, and deoxy-hemoglobin content, some researchers tried to use NIOI to reveal the nature of the BOLD signal. Rat studies using 2D optical imaging (Devor et al., 2003) showed the non-linear mapping between the neuronal activity and evoked hemodynamic processes. This result should be a red flag for those who try to define the general relation between neuronal activation and BOLD signal as mostly linear. The conjoint analysis of BOLD and NIOI signals revealed the silent BOLD signal during present neural activation registered by E/MEG modalities (Seiyama et al., 2004). This mismatch between E/MEG and fMRI results is known

as the *sensory motor paradox* (Paulesu et al., 1997). To explain this effect, the *Vein and Capillary* model was used to describe the BOLD signal in terms of hemodynamic parameters (Seiyama et al., 2004). The suggested model permits the existence of silent and negative BOLD responses during positive neuronal activation. This fact, together with an increasing number of studies (Stefanovic et al., 2004) confirming that sustained negative BOLD HR is a primary indicator of decreased neuronal activation, provide yet more evidence that the BOLD HR generally is not a simple linear function of neuronal activation but at best is a monotone function which has close to linear behavior in a wide range of nuisance neurophysiologic parameters. We conclude this section by noting that the absence of a generative model of the BOLD response prevents the development of universal methods of multimodal analysis. Nevertheless, as discussed in this section and is shown by the results presented in the next section, there are specific ranges of applications where the linearity between BOLD and neuronal activation can be assumed.

### 8.4.3 Analysis Methods

Whenever applicable, a simple comparative analysis of the results obtained from the conventional uni-modal analyses together with findings reported elsewhere, can be considered as the first confirmatory level of a multimodal analysis. This type of analysis is very flexible, as long as the researcher knows how to interpret the results and to draw useful conclusions, especially whenever the results of comparison reveal commonalities and differences between the two (Vitacco et al., 2002). On the other hand, by default a unimodal analysis makes limited use of the data from the modalities, and encourages researchers to look for analysis methods which would incorporate the advantages of each single modality. Nevertheless, simple inspection is helpful for drawing preliminary conclusions on the plausibility to perform any conjoint analysis using one of the methods described in this section, including correlative analysis which might be considered an initial approach to try.

#### Correlative Analysis of EEG and MEG with fMRI

In some experiments, the E/MEG signal can serve as the detector of spontaneous neuronal activity (*e.g.* epileptic discharges) or changes in the processing states (*e.g.* vigilance states). The time onsets derived from E/MEG are alone valuable for further fMRI analysis, where the BOLD signal often cannot provide such timing information. For instance, such use of EEG data is characteristic for the experiments performed via a *Triggered fMRI* acquisition scheme (Section 8.3.2).

Correlative E/MEG/fMRI analysis becomes more intriguing if there is a stronger belief in the linear dependency between the BOLD response and features of E/MEG signal (*e.g.* amplitudes of ERP peaks, powers of frequency components), than between the hemodynamics of the brain and the corresponding parameter of the design (*e.g.* frequency of stimulus presentation or level of stimulus degradation). Then E/MEG/fMRI analysis effectively reduces the inherent bias present in the conventional fMRI analysis methods by removing the possible non-linearity between the design parameter and the evoked neuronal response.

The correlative analysis relies on the preprocessing of E/MEG data to extract the features of interest to be compared with the fMRI time course. The obtained E/MEG features first get convolved with a hypothetical HRF (Section 8.4.2) to accommodate for the HR sloppiness and are then subsampled to fit the temporal resolution of fMRI. The analysis of fMRI signal correlation with amplitudes of selected peaks of ERPs revealed sets of voxels which have a close to linear dependency between the BOLD response and amplitude of the selected ERP peak (N170 in Horovitz et al. (2004), P300 in Horovitz et al. (2002), and amplitude of mismatch negativity (MMN) (Liebenthal et al., 2003)), thus providing a strong correlation ($P < 0.001$ (Horovitz et al., 2004)). A parametric experimental design with different noise levels introduced for the stimulus degradation (Liebenthal et al., 2003; Horovitz et al., 2004) or different levels of sound frequency deviant (Liebenthal et al., 2003) helped to extend the range of detected ERP and fMRI activations, thus effectively increasing the significance of the results found. To

support the suggested connection between the specific ERP peak and fMRI activated area, the correlation of the same BOLD signal with the other ERP peaks must be lower if any at all (Horovitz et al., 2004). As a consequence, such analysis cannot prove that any specific peak of EEG is produced by the neurons located in the fMRI detected areas alone but it definitely shows that they are connected in the specific paradigm.

The search for the covariates between the BOLD signal and wide-spread neuronal signals, such as the alpha rhythm, remains a more difficult problem due to the ambiguity of the underlying process, since there are many possible generators of alpha rhythms corresponding to various functions (Niedermeyer, 1997). As an example, Goldman et al. (2002) and Laufs et al. (2003a) were looking for the dependency between fMRI signal and EEG alpha rhythm power during interleaved and simultaneous EEG/fMRI acquisition correspondingly. They report similar (negative correlation in parietal and frontal cortical activity), as well as contradictory (positive correlation) findings, which can be explained by the variations in the experimental setup (Laufs et al., 2003b) or by the heterogeneous coupling between the alpha rhythm and the BOLD response (Laufs et al., 2003a). Despite the obvious simplification of the correlative methods, they may still have a role to play in constraining and revealing the definitive forward model in multimodal applications.

### Decomposition Techniques

The common drawback of the presented correlative analyses techniques is that they are based on the selection of the specific feature of the E/MEG signal to be correlated with the fMRI time trends, which are not so perfectly conditioned to be characterized primarily by the feature of interest. The variance of the background processes, which are present in the fMRI data and are possibly explained by the discarded information from the E/MEG data, can reduce the significance of the found correlation. That is why it was suggested (Martinez-Montes et al., 2004) to use the entirety of the E/MEG signal, without focusing on its specific frequency band, to derive the E/MEG and fMRI signal components which have the strongest correlation among them. The introduction of decomposition techniques (such as basis pursuit, PCA, ICA, *etc.*) into the multimodal analysis makes this work particularly interesting.

To perform the decomposition (Martinez-Montes et al., 2004), Partial Least-Squares (PLS) regression was generalized into the tri-PLS2 model, which represents the E/MEG spectrum as a linear composition of trilinear components. Each component is the product of spatial (among E/MEG sensors), spectral and temporal factors, where the temporal factors have to be maximally correlated with the corresponding temporal component of the similar fMRI signal decomposition into bilinear components: products of the spatial and temporal factors. Analysis using tri-PLS2 modeling on the data from Goldman et al. (2002) found a decomposition into 3 components corresponding to alpha, theta and gamma bands of the EEG signal. The fMRI components found had a strong correlation only in alpha band component (Pearson correlation $0.83$ ($p = 0.005$)), although the theta component also showed a linear correlation of $0.56$ ($p = 0.070$). It is interesting to note, that spectral profiles of the trilinear EEG atoms received with and without fMRI influence were almost identical, which can be explained either by the non-influential role of fMRI in tri-PLS2 decomposition of EEG, or just by a good agreement between the two. On the other hand, EEG definitely guided fMRI decomposition, so that the alpha rhythm spatial fMRI component agreed very well with the previous findings (Goldman et al., 2002).

### Equivalent Current Dipole Models

ECD is the most elaborated and widely used technique for source localization in EMSI. It can easily account for activation areas obtained from the fMRI analysis thus giving the necessary fine time-space resolution by minimizing the search space of non-linear optimization to the thresholded fMRI activation map. While being very attractive, such a method bears most of the problems of the ECD method mentioned in Section 8.2.3, and

introduces another possible bias due to the belief in the strong coupling between hemodynamic and electrophysiological activities. For this reason it needs to be approached with caution in order to carefully select the fMRI regions to be used in the ECD/fMRI combined analysis.

Although good correspondence between ECD and fMRI results is often found (Ahlfors et al., 1999), some studies reported a significant (1–5 cm) displacement between locations obtained from fMRI analysis and ECD modeling (Beisteiner et al., 1997; Korvenoja et al., 1999; Lemieux et al., 2001; Gonzalez Andino et al., 2001). It is interesting to note, that such displacement can be very consistent across the experiments of different researchers using the same paradigm (for instance motor activations (Korvenoja et al., 1999; Kober et al., 2001; Schulz et al., 2004)). As it was already mentioned, in the first step, a simple comparison of detected activations across the two modalities can be done to increase the reliability of dipole localization alone. Further, additional weighting by the distance from the ECD to the corresponding fMRI activation foci can guide ECD optimization (Wagner and Fuchs, 2001) and silent in fMRI activations can be accommodated by introducing free dipoles without the constraint on dipole location.

Auxiliary fMRI results can help to resolve the ambiguity of the inverse E/MEG problem if ECD lies in the neighborhood of multiple fMRI activations. Placing multiple ECDs inside the fMRI foci with successive optimization of ECDs orientations and magnitudes may produce more meaningful results, especially if it better describes the E/MEG signal by the suggested multiple ECDs model.

Due the large number of consistent published fMRI results, it seems viable to perform a pure E/MEG experiment with consequent ECD analysis using known relevant fMRI activation areas found by the other researchers performing the same kind of experiment (Foxe et al., 2003), thus providing the missing temporal explanation to the known fMRI activations.

### Linear Inverse Methods

Dale and Sereno (1993) formulated a simple but powerful linear framework for the integration of different imaging modalities into the inverse solution of DECD, where the solution was presented as unregularized (just minimum-norm) (8.8) with $\mathbf{W_Q} = \mathbf{C}_S$ and $\lambda \mathbf{W_X} = \mathbf{C}_\epsilon$. The simplest way to account for fMRI data is to use thresholded fMRI activation map as the inverse solution space but this was rejected (George et al., 1995b) due to its incapability to account for fMRI silent sources, which is why the idea to incorporate variance information from fMRI into $\mathbf{C}_S$ was further elaborated (Liu et al., 1998) by the introduction of relative weighting for fMRI activated voxels via constructing a diagonal matrix $\mathbf{W_Q} = \mathbf{W}_{\text{fMRI}} = \{\nu_{ii}\}$, where $\nu_{ii} = 1$ for fMRI activated voxels and $\nu_{ii} = \nu_0 \in [0, 1]$ for voxels which are not revealed by fMRI analysis. A Monte Carlo simulation showed that $\nu_0 = 0.1$ (which corresponds to the $90\%$ relative fMRI weighting) leads to a good compromise with the ability to find activation in the areas which are not found active by fMRI analysis and to detect active fMRI spots (even superficial) in the DECD inverse solution. An alternative formulation of the relative fMRI weighting in the DECD solution can be given using a subspace regularization (SSR) technique (Ahlfors and Simpson, 2004), in which an E/MEG source estimate is chosen from all possible solutions describing the E/MEG signal, and is such that it minimizes the distance to a subspace defined by the fMRI data (Fig. 8.2). Such formulation helps to understand the mechanism of fMRI influence on the inverse E/MEG solution: SSR biases underdetermined the E/MEG source locations toward the fMRI foci.

The relative fMRI weighting was tested (Dale et al., 2000) in an MEG experiment and found conjoint fMRI/MEG analysis results similar to the results reported in previous fMRI, PET, MEG and intracranial EEG studies. Babiloni et al. (2001) followed Dale et al. (2000) in a high resolution EEG and fMRI study to incorporate non-thresholded fMRI activation maps with other factors. First of all, the $\mathbf{W}_{\text{fMRI}}$ was reformulated to $(\mathbf{W}_{\text{fMRI}\prime})_{ii} = \nu_0 + (1 - \nu_0)\Delta_i/\Delta_{\max}$, where $\Delta_i$ corresponds to the relative change of the fMRI signal in the $i$-th voxel, and $\Delta_{\max}$ is the maximal detected change. This way the relative E/MEG/fMRI scheme is preserved and locations of stronger fMRI activations have higher prior variance. Finally the three available weight-

ing factors were combined: fMRI relative weighting, correlation structure obtained from fMRI described by the matrix of correlation coefficients $\mathbf{K}_S$, and the gain normalization weighting matrix $\mathbf{W}_{\text{n}}$ (Section 8.2.3): $\mathbf{W}_{\mathbf{Q}} = \mathbf{W}_{\text{fMRI}\prime}^{1/2}\mathbf{W}_{\text{n}}^{1/2}\mathbf{K}_S\mathbf{W}_{\text{n}}^{1/2}\mathbf{W}_{\text{fMRI}\prime}^{1/2}$. Although $\mathbf{W}_{\text{fMRI}\prime}$ alone had improved EMSI localization, the incorporation of the $\mathbf{K}_S$ lead to finer localization of neuronal activation associated with finger movement.

Although most of the previously discussed DECD methods are involved in finding minimal $L_2$ norm solution, the fMRI conditioned solution with minimal $L_1$ norm (regularization term in (8.6) $f(\mathbf{Q}) = \|\mathbf{Q}\|_1$) is shown to provide a sparser activation map (Fuchs et al., 1999) with activity focalized to the seeded hotspot locations (Wagner and Fuchs, 2001).

An fMRI-conditioned linear inverse is an appealing method due to its simplicity, and rich background of DECD linear inverse methods derived for the analysis of E/MEG signals. Nonetheless, one should approach these methods with extreme caution in a domain where non-linear coupling between BOLD and neural activity is likely to overwhelm any linear approximation (Gonzalez Andino et al., 2001).

### Beamforming

Lahaye et al. (2004) suggest an iterative algorithm for conjoint analysis of EEG and fMRI data acquired simultaneously during an event-related experiment. Their method relies on iterated source localization by the LCMV beamformer (8.10), which makes use of both EEG and fMRI data. The covariance $\mathbf{C}_X$ used by the beamformer is calculated anew each time step, using the previously estimated sources and current event responses from both modalities. This way neuronal sites with a good agreement between the BOLD response and EEG beamformer reconstructed source amplitude, benefit most at each iteration. Although the original formulation is cumbersome, this method appears promising as (a) it makes use of both spatial and temporal information available from both modalities, and (b) it can account for silent BOLD sources using an electro-metabolic coupling constant which is estimated for each dipole and defines the influence of the BOLD signal at a given location onto the estimation of $\mathbf{C}_S$ which, in turn, drives the estimate of $\mathbf{C}_X$.

### Bayesian Inference

During the last decade, Bayesian methods became dominant in the probabilistic signal analysis. The idea behind them is to use Bayes' rule to derive a *posterior probability* of a given *hypothesis* having observed data $\mathcal{D}$, which serves as *evidence* to support the hypothesis

$$p(\mathcal{H}|\mathcal{D}) = \frac{p(\mathcal{D}|\mathcal{H})\, p(\mathcal{H})}{p(\mathcal{D})}, \tag{8.18}$$

where $p(\mathcal{H})$ and $p(\mathcal{D})$ are prior probabilities of the hypothesis and evidence correspondingly, and the conditional probability $p(\mathcal{D}|\mathcal{H})$ is known as a *likelihood function*. Thus, (8.18) can be viewed as a method to combine the results of conventional likelihood analyses for multiple hypotheses into the posterior probability of the hypotheses $p(\mathcal{H}|\mathcal{D})$ or some function of it, after been exposed to the data. The derived posterior probability can be used to select the most probable hypothesis, *i.e.* the one with the highest probability

$$\hat{\mathcal{H}}_{|\mathcal{D}} = \arg\max_{\mathcal{H}} p(\mathcal{H}|\mathcal{D}) = \arg\max_{\mathcal{H}} \log p(\mathcal{D}|\mathcal{H}) + \log p(\mathcal{H}) \tag{8.19}$$

leading to the maximum *a posteriori* (MAP) estimate, where the prior data probability $p(\mathcal{D})$ (often called a *partition function*) is omitted because the data does not depend on the choice of the hypothesis and it does not influence the maximization over $\mathcal{H}$.

For the class of problems related to the signal processing, hypothesis $\mathcal{H}$ generally consists of a model $\mathcal{M}$ characterized by a set of nuisance parameters $\mathbf{\Theta} = \{\theta_1, \theta_{2\ldots n}\}$. The primary goal usually is to find a MAP estimate

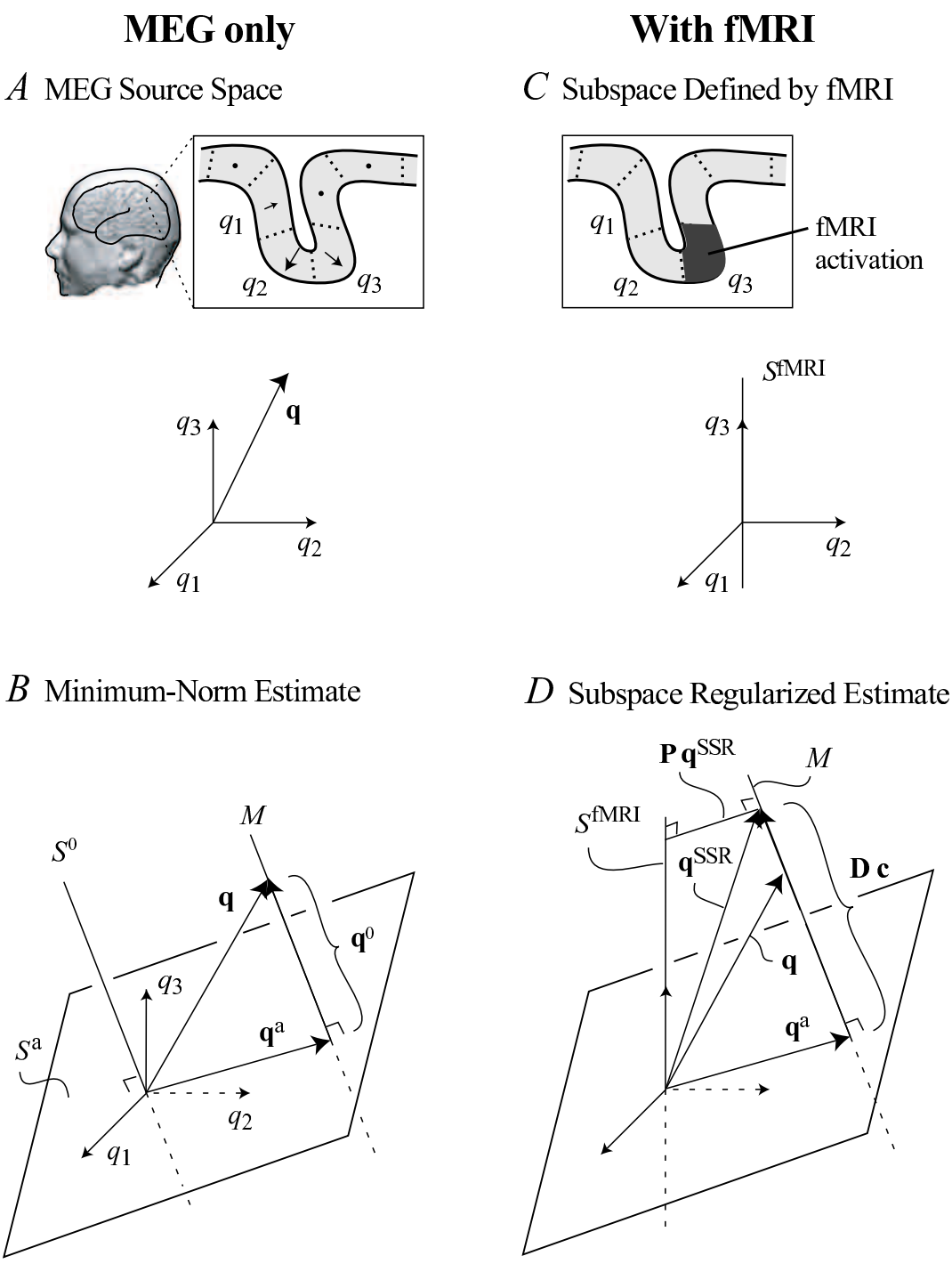


Figure 8.2: Geometrical interpretation of subspace regularization in the MEG/EEG source space. (A) The cerebral cortex is divided into source elements $\mathbf{q}_1, \mathbf{q}_2, \ldots, \mathbf{q}_K$, each representing an ECD with a fixed orientation. All source distributions compose a vector $\mathbf{q}$ in $K$-dimensional space. (B) The source distribution $\mathbf{q}$ is divided into two components $\mathbf{q}^a \in S^{\mathrm{a}} \equiv \mathrm{range}(\mathbf{G}^\top)$, determined by the sensitivity of MEG sensors and $\mathbf{q}^0 \in \mathrm{null}\,\mathbf{G}$, which does not produce an MEG signal. (C) The fMRI activations define another subspace $S^{\mathrm{fMRI}}$. (D) The subspace-regularized fMRI-guided solution $\mathbf{q}^{\mathrm{SSR}} \in \mathrm{M}$ is closest to $S^{\mathrm{fMRI}}$, minimizing the distance $\|\mathbf{P}\mathbf{q}^{\mathrm{SSR}}\|$, where $\mathbf{P}$ (a $N \times N$ diagonal matrix with $\mathbf{P}_{ii} = 1/0$ when the $i$-th fMRI voxel is active/inactive) is the projection matrix into the orthogonal complement of $S^{\mathrm{fMRI}}$. (Adapted from Ahlfors and Simpson (2004, Figure 1), with permission.)

of some quantity of interest $\mathbf{\Delta}$ or, more generally, its posterior probability distribution $p(\mathbf{\Delta}|\mathcal{D}, \mathcal{M}, \mathbf{\Theta})$. $\mathbf{\Delta}$ can be an arbitrary function of the hypothesis or its components $\mathbf{\Delta} = f(\mathcal{H})$, or often just a specific nuisance parameter of the model $\mathbf{\Delta} \equiv \theta_1$. To obtain posterior probability of the nuisance parameter, its marginal probability has to be computed by the integration over the rest of the parameters of the model

$$p(\theta_1|\mathcal{D}, \mathcal{M}) = \int p(\theta_1, \theta_{2\ldots n}|\mathcal{D}, \mathcal{M})\, d\theta_{2\ldots n} = \int p(\theta_1|\theta_{2\ldots n}, \mathcal{D}, \mathcal{M})\, p(\theta_{2\ldots n}|\mathcal{D}, \mathcal{M})\, d\theta_{2\ldots n}. \tag{8.20}$$

Due to the integration operation involved in determination of any marginal probability, Bayesian analysis becomes very computationally intensive if analytical integral solution does not exist. Therefore, sampling techniques (*e.g.* MCMC, Gibbs sampler) are often used to estimate full posterior probability $p(\mathbf{\Delta}|\mathcal{D}, \mathcal{M})$, MAP $\hat{\mathbf{\Delta}}_{|\mathcal{D},\mathcal{M}} = \arg\max_{\mathbf{\Delta}} p(\mathbf{\Delta}|\mathcal{D}, \mathcal{M})$, or some statistics such as an expected value $E[\mathbf{\Delta}|\mathcal{D}, \mathcal{M}]$ of the quantity of interest.

The Bayesian approach sounds very appealing for the development of multimodal methods. It is inherently able to incorporate all available evidence, which is in our case obtained from the fMRI and E/MEG data ($\mathcal{D} = \{\mathbf{X}, \mathbf{B}\}$) to support the hypothesis on the location of neuronal activations, which is in the case of DECD model is $\mathcal{H} = \{\mathbf{Q}, \mathcal{M}\}$. However, the detailed analysis of (8.18) leads to necessary simplifications and assumptions of the prior probabilities in order to derive a computationally tractable formulation. Therefore it often loses its generality. Thus to derive a MAP estimator for $\hat{\mathbf{Q}}_{|\mathbf{X},\mathbf{B},\mathcal{M}}$ Trujillo-Barreto et al. (2001) had to condition the computation by a set of simplifying modeling assumptions such as: noise is normally distributed, nuisance parameters of forward models have inverse Gamma prior distributions, and neuronal activation is described by a linear function of hemodynamic response. The results on simulated and experimental data from a somatosensory MEG/fMRI experiment confirmed the applicability of Bayesian formalism to the multimodal imaging even under the set of simplifying assumptions mentioned above.

Usually, model $\mathcal{M}$ is not explicitly mentioned in Bayesian formulations (such as (8.20)) because only a single model is considered. For instance, Bayesian formulation of LORETA E/MEG inverse corresponds to a DECD model, where $\mathbf{\Theta} = \mathbf{Q}$ is constrained to be smooth (in space), and to cover whole cortex surface. In the case of the *Bayesian Model Averaging* (BMA), the analysis is carried out for different models $\mathcal{M}_i$, which might have different nuisance parameters, *e.g.* E/MEG and BOLD signals forward models, possible spatial locations of the activations, constraints to regularize E/MEG inverse solutions. In BMA analysis we combine results obtained using all considered models to compute the posterior distribution of the quantity of interest

$$p(\mathbf{\Delta}|\mathcal{D}) = \sum_i p(\mathbf{\Delta}|\mathcal{D}, \mathcal{M}_i)\, p(\mathcal{M}_i|\mathcal{D}), \tag{8.21}$$

where the posterior probability $p(\mathcal{M}_i|\mathcal{D})$ of any given model $\mathcal{M}_i$ is computed via Bayes' rule using prior probabilities $p(\mathcal{M}_i)$, $p(\mathcal{D})$ and the likelihood of the data given each model

$$p(\mathcal{D}|\mathcal{M}_i) = \int p(\mathcal{D}|\mathbf{\Theta}, \mathcal{M}_i)\, p(\mathbf{\Theta}|\mathcal{M}_i)\, d\mathbf{\Theta}. \tag{8.22}$$

Initially, BMA was introduced into the E/MEG imaging (Trujillo-Barreto et al., 2004), where Bayesian interpretation of (8.8) was formulated to obtain $p(\mathbf{Q}|\mathbf{X}, \mathbf{B})$ for the case of Gaussian uncorrelated noise ($\mathbf{W}_{\mathbf{X}} = \mathbf{C}_\epsilon = \nu_\epsilon \mathbf{I}$). In order to create a model, we partition the brain volume into a limited set of spatially distinct functional compartments, which are arbitrarily combined to define a $\mathcal{M}_i$, search space for the E/MEG inverse problem.

At the end, different models are sampled from the posterior probability $p(\mathcal{M}_i|\mathbf{X})$ to get the estimate of the expected activity distribution of ECDs over all considered source models

$$E[\mathbf{Q}|\mathbf{X}] = \sum_i E[\mathbf{Q}|\mathbf{X}, \mathcal{M}_i]\, p(\mathcal{M}_i|\mathbf{X})$$

$$\mathrm{Var}[\mathbf{Q}|\mathbf{X}] = \sum_i \mathrm{Var}[\mathbf{Q}|\mathbf{X}, \mathcal{M}_i]\, p(\mathcal{M}_i|\mathbf{X}),$$

where the normalized probability $p(\mathcal{M}_i|\mathbf{X})$, Bayes' Factor $B_{i0}$, and prior odds $\alpha_i$, are

$$p(\mathcal{M}_i|\mathbf{X}) = \frac{\alpha_i B_{i0}}{\sum_k \alpha_k B_{k0}} \qquad B_{i0} = \frac{p(\mathbf{X}|\mathcal{M}_i)}{p(\mathbf{X}|\mathcal{M}_0)} \qquad \alpha_i = \frac{p(\mathcal{M}_i)}{p(\mathcal{M}_0)}$$

In the original BMA framework for E/MEG (Trujillo-Barreto et al., 2004) $\alpha_i = 1 \,\forall i$, *i.e.* the models had a flat prior PDF because no additional functional information was available at that point. Melie-García et al. (2004) suggested to use the significance values of fMRI statistical t-maps to derive $p(\mathcal{M}_i)$ as the mean of all such significance probabilities across the present in $\mathcal{M}_i$ compartments. This strategy causes the models consisting of the compartments with significantly activated voxels get higher prior probabilities in BMA. The introduction of fMRI information as the prior to BMA analysis reduced the ambiguity of the inverse solution, thus leading to better localization performance. Although further analysis is necessary to define the applicability range of the BMA in E/MEG/fMRI fusion, it already looks promising because of the use of fMRI information as an additional evidence factor in E/MEG localization rather than a hard constraint.

Due to the flexibility of Bayesian formalism, various Bayesian methods solving E/MEG inverse problem already can be easily extended to partially accommodate evidence obtained from the analysis of fMRI data. For instance, correlation among different areas obtained from fMRI data analysis can be used as a prior in the Bayesian reconstruction of correlated sources (Sahani and Nagarajan, 2004). The development of a neurophysiologic generative model of BOLD signal would allow many Bayesian inference methods (such as Schmidt et al. (1999)) to introduce complete temporal and spatial fMRI information into the analysis of E/MEG data.

## 8.5 Considerations and Future Directions

Although the BOLD signal is inherently non-linear as a function of neuronal activation, there have been multiple reports of linear dependency between the observed BOLD response and the selected set of the E/MEG signal features. In general, such results are not inconsistent with the non-linearity of BOLD, since of course, a non-linear function can be well approximated in a context of a specific experimental design, or regions of interest, or dynamic ranges of the selected features of E/MEG signals. Besides LFP/BOLD linearity reported by Logothetis and confirmed in the specific frequency bands of EEG signal during flashing checkerboard experiment (Singh et al., 2003), there have been reports of a strong correlation between the BOLD signal amplitude and other features of E/MEG responses.

In the past, DC-E/MEG signal have not been of an attention for multimodal integration, despite recent experiments showing the strong correlation between the changes of the observed DC-EEG signal and hemodynamic changes in the human brain (Vanhatalo et al., 2003). In fact, such DC-E/MEG/BOLD coupling suggests that the integration of fMRI and DC-E/MEG might be a particularly useful way to study the nature of the time variations in HR signal which are usually observed during fMRI experiments but are not explicitly explained by the experimental design or the physics of the MR acquisition process.

Many EMSI methods can be naturally extended to account for fMRI data if a generative forward model of BOLD signal is available. For instance, direct universal-approximator inverse methods (Jun et al., 2003; Jun and Pearlmutter, 2005) have been found to be very effective (fast, robust to noise and to complex forward models) for the E/MEG dipole localization problem, and could be augmented to accept fMRI data if the generative model were augmented to produce it.

FMRI conditioned E/MEG DECD methods have been shown to be a relatively simple and mathematically compelling for source imaging when there is good spatial agreement between E/MEG and fMRI signals. Due to the advantages of such methods, it might be valuable to consider other advanced E/MEG DECD methods such

as FOCUSS (Gorodnitsky and Rao, 1997), which is known to bring improvement of estimation of focal sources over simple linear inverse methods (Baillet et al., 2001b).

ICA as a signal decomposition technique has been found effective to remove artifacts in E/MEG without degrading neuronal signals (Vigário et al., 2000; Tang et al., 2000a; Jung et al., 2000a,b), moreover is known to be superior to PCA in the component analysis of E/MEG signals (Jung et al., 1999a). Initial research using ICA of fMRI in the spatial domain (McKeown et al., 1998) was controversial, however consecutive experiments and generalization of ICA to fMRI in the temporal domain (see Calhoun et al. (2003) for an overview) has increased its normative value. The development of ICA methods for the analysis of multimodal data provides a logical extension of the decomposition techniques covered earlier in the chapter.

Since most of the multimodal methods presented in this chapter rely upon the linear dependence between signals, it is important to analyze, expand and formalize the knowledge about the "linear" case. The formulation of a general BOLD signal model capable of describing the desired non-linear dependency in terms of neuronal activation and nuisance physiological parameters would constitute a major step toward the development of the multimodal methods with wider range of application than in the current "linear" domain. Without such a model and without valid estimates of the underlying physiological parameters involved in the model, no multimodal analysis results can be trusted as novel.

In sum, it seems clear that fMRI should serve as a complementary evidence factor, rather than a hard constraint, in E/MEG source localization methods. The preprocessing of both fMRI and E/MEG signals should be done in order to select features of interest which had been previously reported to have good agreement between the two modalities. Any multimodal experiment should be based on the comparative study of unimodal experiments and analyses which show good agreement before performing conjoint data analysis.

Table 8.2: Free software germane to multimodal analysis of EEG/MEG/fMRI data (⇌ stands for Input/Output facility for a feature)

| | **Forward** | | | | | | **EEG/MEG Inverse** | | | **MRI**† | | | | | **fMRI** | **Environment** | | | |
|---|---|---|---|---|---|---|---|---|---|---|---|---|---|---|---|---|---|---|---|
| | **EEG** | | | **MEG** | | | | | | | | | | | | | | | |
| **Package** | Spherical | BEM | FEM | Spherical | BEM | FEM | ECD | DECD | Beamforming | Brain Segmentation | Skull Segmentation | Scalp Segmentation | Tessellation | E/MEG Registration | | Matlab | POSIX‡ | Mac OS X | MS Windows |
| Brainstorm (Leahy et al., 2004) | √ | √ | | √ | √ | | | √ | √ | | | | ⇌ | √ | | √ | | | |
| NeuroFEM (2005)/Pebbles | √ | √ | √ | √ | √ | √ | √ | √ | | | | | ⇌ | | | | √ | √ | |
| BioPSE (2002)/SCIRun (2002) | √ | √ | √ | | | | √ | √ | | | | | ⇌ | | √ | ⇌ | √ | | |
| Brainvisa/Anatomist (Poupon, 1999) | | | | | | | | | | √ | | √ | √ | | √ | | √ | √ | √ |
| FreeSurfer (2004) | | | | | | | | | | √ | | √ | √ | | √ | | √ | √ | |
| Surefit (Van Essen, 2004) | | | | | | | | | | √ | | √ | √ | | √ | | √ | | |
| Brainsuite (Shattuck and Leahy, 2002) | | | | | | | | | | √ | √ | √ | √ | | | | | | √ |
| EEG/MEG/MRI tlbx* (Weber, 2004) | √ | | | √ | | | √ | √ | | ⇌ | ⇌ | ⇌ | ⇌ | √ | √ | √ | | | |
| MEG tlbx* (Moran, 2005) | | | | √ | | | √ | √ | | √ | √ | √ | √ | √ | √ | √ | | | |
| EEGLAB/FMRILAB (Delorme and Makeig, 2004) | | | | | | | √ | | | | | | | | √ | √ | | | |

†An extensive MR segmentation bibliography is available online (Nielsen, 2001).

‡POSIX includes all versions of Unix and GNU/Linux. Most POSIX packages listed use X Windows for their graphical output.

*Matlab Toolbox.

# References


Adjamian, P., Barnes, G. R., Hillebrand, A., Holliday, I. E., Singh, K. D., Furlong, P. L., Harrington, E., Barclay, C. W., and Route, P. J. (2004). Co-registration of magnetoencephalography with magnetic resonance imaging using bite-bar-based fiducials and surface-matching. *Clin Neurophysiol*, 115(3):691–698.

Ahlfors, S. P. and Simpson, G. V. (2004). Geometrical interpretation of fMRI-guided MEG/EEG inverse estimates. *NeuroImage*, 22(1):323–332.

Ahlfors, S. P., Simpson, G. V., Dale, A. M., Belliveau, J. W., Liu, A. K., Korvenoja, A., Virtanen, J., Huotilainen, M., Tootell, R. B., Aronen, H. J., and Ilmoniemi, R. J. (1999). Spatiotemporal activity of a cortical network for processing visual motion revealed by MEG and fMRI. *J Neurophysiol*, 82(5):2545–2555.

Allen, P. J., Josephs, O., and Turner, R. (2000). A method for removing imaging artifact from continuous EEG recorded during functional MRI. *NeuroImage*, 12(2):230–239.

Anami, K., Mori, T., Tanaka, F., Kawagoe, Y., Okamoto, J., Yarita, M., Ohnishi, T., Yumoto, M., Matsuda, H., and Saitoh, O. (2003). Stepping stone sampling for retrieving artifact-free electroencephalogram during functional magnetic resonance imaging. *NeuroImage*, 19(2.1):281–295.

Angelone, L. M., Potthast, A., Segonne, F., Iwaki, S., Belliveau, J. W., and Bonmassar, G. (2004). Metallic electrodes and leads in simultaneous EEG-MRI: specific absorption rate (SAR) simulation studies. *Bioelectromagnetics*, 25(4):285–295.

Arthurs, O. J. and Boniface, S. (2002). How well do we understand the neural origins of the fMRI BOLD signal? *Trends Neurosci*, 25(1):27–31.

Attwell, D. and Iadecola, C. (2002). The neural basis of functional brain imaging signals. *Trends Neurosci*, 25(12):621–625.

Babiloni, F., Babiloni, C., Carducci, F., Angelone, L., Del-Gratta, C., Romani, G. L., Rossini, P. M., and Cincotti, F. (2001). Linear inverse estimation of cortical sources by using high resolution EEG and fMRI priors. *Int. J. of Bioelectromag.*, 3(1).

Backus, G. and Gilbert, F. (1968). The resolving power of gross Earth data. *Geophys. J. R. Astron. Soc.*, 16:169–205.

Baillet, S. and Garnero, L. (1997). A bayesian approach to introducing anatomo-functional priors in the EEG/MEG inverse problem. *IEEE Trans. Biomed. Eng.*, 44(5):374–385.

Baillet, S., Garnero, L., Marin, G., and Hugonin, J. P. (1999). Combined MEG and EEG source imaging by minimization of mutual information. *IEEE Transactions on Biomedical Engineering*, 46(5):522–534.

Baillet, S., Mosher, J. C., and Leahy, M. (2001a). Electromagnetic brain mapping. *IEEE Sig Proc Mag*, 18(6):14–30.

Baillet, S., Riera, J., Marin, G., Mangin, J., Aubert, J., and Garnero, L. (2001b). Evaluation of inverse methods and head models for EEG source localization using a human skull phantom. *Phys Med Biol*, 46(1):77–96.

Beisteiner, R., Erdler, M., Teichtmeister, C., Diemling, M., Moser, E., Edward, V., and Deecke, L. (1997). Magnetoencephalography may help to improve functional MRI brain mapping. *Eur J Neurosci*, 9(5):1072–1077.

BioPSE (2002). Problem solving environment for modeling, simulation, and visualization of bioelectric fields. Scientific Computing and Imaging Institute (SCI).

Bodurka, J. and Bandettini, P. A. (2002). Toward direct mapping of neuronal activity: MRI detection of ultraweak, transient magnetic field changes. *Magn Reson Med*, 47(6):1052–1058.

Bonmassar, G., Purdon, P. L., Jaaskelainen, I. P., Chiappa, K., Solo, V., Brown, E. N., and Belliveau, J. W. (2002). Motion and ballistocardiogram artifact removal for interleaved recording of EEG and EPs during MRI. *NeuroImage*, 16(4):1127–1141.

Bonmassar, G., Schwartz, D. P., Liu, A. K., Kwong, K. K., Dale, A. M., and Belliveau, J. W. (2001). Spa-

tiotemporal brain imaging of visual-evoked activity using interleaved EEG and fMRI recordings. *NeuroImage*, 13(6.1):1035–1043.

Boynton, G. M., Engel, S. A., Glover, G. H., and Heeger, D. J. (1996). Linear systems analysis of functional magnetic resonance imaging in human V1. *J Neurosci*, 16(13):4207–4221.

Brazier, M. A. B. (1949). A study of the electric field at the surface of the head. *Electroencephalogr. Clin. Neurophysiol.*, 2:38–52.

Brooks, D. H., Ahmad, G. F., MacLeod, R. S., and Maratos, G. M. (1999). Inverse electrocardiography by simultaneous imposition of multiple constraints. *IEEE Trans Biomed Eng*, 46(1):3–18.

Buxton, R. B. and Frank, L. R. (1997). A model for the coupling between cerebral blood flow and oxygen metabolism during neural stimulation. *J Cereb Blood Flow Metab*, 17(1):64–72.

Calhoun, V. D., Adali, T., Hansen, L. K., Larsen, J., and Pekar, J. J. (2003). ICA of functional MRI data: An overview. In *Fourth International Symposium on Independent Component Analysis and Blind Source Separation*, pages 281–288, Nara, Japan. Invited Paper.

Castellano, S. A. (1999). *The Folding of the Human Brain: From Shape to Function*. PhD thesis, University of London, Division of Radiological Sciences and Medical Engineering, King's College London.

Ciuciu, P., Poline, J. B., Marrelec, G., Idier, J., Pallier, C., and Benali, H. (2003). Unsupervised robust nonparametric estimation of the hemodynamic response function for any fMRI experiment. *IEEE Trans Med Imaging*, 22(10):1235–1251.

Cohen, D. (1972). Magnetoencephalography: detection of the brain's electrical activity with a superconducting magnetometer. *Science*, 175:664–666.

Cohen, D. and Halgren, E. (2003). Magnetoencephalography (neuromagnetism). In *Encyclopedia of Neuroscience*, pages 1–7. Elsevier, 3rd edition.

Cohen, M. S. (1997). Parametric analysis of fMRI data using linear systems methods. *NeuroImage*, 6(2):93–103.

Cohen, M. S. (2004). Method and apparatus for reducing contamination of an electrical signal. United States Patent application 0040097802.

Cohen, M. S., Goldman, R. I., Stern, J., and Engel, Jr., J. (2001). Simultaneous EEG and fMRI made easy. *NeuroImage*, 13(6 Supp.1):S6.

Dale, A. M., Fischl, B., and Sereno, M. I. (1999). Cortical surface-based analysis. I. Segmentation and surface reconstruction. *NeuroImage*, 9(2):179–194.

Dale, A. M., Liu, A. K., Fischl, B., Lewine, J. D., Buckner, R. L., Belliveau, J. W., and Halgren, E. (2000). Dynamic statistical parameter mapping: combining fMRI and MEG to produce high resolution imaging of cortical activity. *Neuron*, 26:55–67.

Dale, A. M. and Sereno, M. I. (1993). Improved localization of cortical activity by combining EEG and MEG with MRI cortical surface reconstruction: A linear approach. *J. of Cog. Neurosci.*, 5(2):162–176.

Delorme, A. and Makeig, S. (2004). EEGLAB: an open source toolbox for analysis of single-trial EEG dynamics including independent component analysis. *J Neurosci Methods*, 134(1):9–21.

Devor, A., Dunn, A. K., Andermann, M. L., Ulbert, I., Boas, D. A., and Dale, A. M. (2003). Coupling of total hemoglobin concentration, oxygenation, and neural activity in rat somatosensory cortex. *Neuron*, 39(2):353–359.

Foucher, J., Otzenberger, H., and Gounot, D. (2004). Where arousal meets attention: a simultaneous fMRI and EEG recording study. *Neuroimage*, 22(2):688–697.

Foxe, J. J., McCourt, M. E., and Javitt, D. C. (2003). Right hemisphere control of visuospatial attention: line-bisection judgments evaluated with high-density electrical mapping and source analysis. *NeuroImage*, 19(3):710–726.

FreeSurfer (2004). FreeSurfer. CorTechs and the Athinoula A. Martinos Center for Biomedical Imaging.

Friston, K. J., Jezzard, P., and Turner, R. (1994). Analysis of functional MRI time-series. *Hum. Brain. Mapp.*,

1:153–171.

Fuchs, M., Wagner, M., Kohler, T., and Wischmann, H. (1999). Linear and nonlinear current density reconstructions. *J Clin Neurophysiol*, 16(3):267–295.

Garreffa, G., Carni, M., Gualniera, G., Ricci, G. B., Bozzao, L., De Carli, D., Morasso, P., Pantano, P., Colonnese, C., Roma, V., and Maraviglia, B. (2003). Real-time MR artifacts filtering during continuous EEG/fMRI acquisition. *Magn Reson Imaging*, 21(10):1175–1189.

Geddes, L. A. and Baker, L. E. (1967). The specific resistance of biological material–a compendium of data for the biomedical engineer and physiologist. *Med Biol Eng*, 5(3):271–293.

George, J. S., Aine, C. J., Mosher, J. C., Schmidt, D. M., Ranken, D. M., Schlitt, H. A., Wood, C. C., Lewine, J. D., Sanders, J. A., and Belliveau, J. W. (1995a). Mapping function in the human brain with magnetoencephalography, anatomical magnetic-resonance-imaging, and functional magnetic-resonance-imaging. *J Clin Neurophysiol*, 12(5):406–431.

George, J. S., Aine, C. J., Mosher, J. C., Schmidt, D. M., Ranken, D. M., Schlitt, H. A., Wood, C. C., Lewine, J. D., Sanders, J. A., and Belliveau, J. W. (1995b). Mapping function in the human brain with magnetoencephalography, anatomical magnetic-resonance-imaging, and functional magnetic-resonance-imaging. *J. of Clin. Neurophysiol.*, 12(5):406–431.

George, J. S., Schmidt, D. M., Rector, D. M., and Wood, C. C. (2002). *Functional MRI: An Introduction to Methods*, chapter 19. Dynamic functional neuroimaging intergratin multiple modalities, pages 353–382. Oxford University Press.

Gitelman, D. R., Penny, W. D., Ashburner, J., and Friston, K. J. (2003). Modeling regional and psychophysiologic interactions in fMRI: the importance of hemodynamic deconvolution. *NeuroImage*, 19(1):200–207.

Glover, G. H. (1999). Deconvolution of impulse response in event-related BOLD fMRI. *NeuroImage*, 9(4):416–429.

Goldman, R. I., Stern, J. M., Engel, Jr, J., and Cohen, M. S. (2000). Acquiring simultaneous EEG and functional MRI. *Clin Neurophysiol*, 111(11):1974–1980.

Goldman, R. I., Stern, J. M., Engel, Jr, J., and Cohen, M. S. (2002). Simultaneous EEG and fMRI of the alpha rhythm. *Neuroreport*, 13(18):2487–2492.

Golub, G., Heath, M., and Wahba, G. (1979). Generalized cross-validation as a method for choosing a good ridge parameter. *Technometrics*, 21:215–223.

Goncalves, S. I., de Munck, J. C., Verbunt, J. P., Bijma, F., Heethaar, R. M., and Lopes da Silva, F. (2003). In vivo measurement of the brain and skull resistivities using an EIT-based method and realistic models for the head. *IEEE Trans Biomed Eng*, 50(6):754–767.

Gonzalez Andino, S. L., Blanke, O., Lantz, G., Thut, G., and Grave de Peralta Menendez, R. (2001). The use of functional constraints for the neuroelectromagnetic inverse problem: Alternatives and caveats. *Int. J. of Bioelectromag.*, 3(1).

Gorodnitsky, I. F. and Rao, B. D. (1997). Sparse signal reconstruction from limited data using FOCUSS: A re-weighted minimum norm algorithm. *IEEE Trans. Signal Proccessing*, 45(3):600–616.

Grave de Peralta Menendez, R. and Gonzalez Andino, S. L. (1998). A critical analysis of linear inverse solutions to the neuroelectromagnetic inverse problem. *IEEE Trans. Biomed. Eng.*, pages 440–448.

Grave de Peralta Menendez, R., Murray, M. M., Michel, C. M., Martuzzi, R., and Gonzalez Andino, S. L. (2004). Electrical neuroimaging based on biophysical constraints. *NeuroImage*, 21(2):527–539.

Hämäläinen, M., Hari, R., Ilmoniemi, R. J., Knuutila, J., and Lounasmaa, O. V. (1993). Magnetoencephalography—theory, instrumentation, and applications to noninvasive studies of the working human brain. *Rev. Modern Physics*, 65(2):413–497.

Hamalainen, M. S. and Sarvas, J. (1989). Realistic conductivity geometry model of the human head for interpretation of neuromagnetic data. *IEEE Trans Biomed Eng*, 36(2):165–171.

Hansen, P. C. (1992). Analysis of discrete ill-posed problems by means of the L-curve. In *SIAM Review*, volume 34, pages 561–580. Society for Industrial and Applied Mathematics, Philadelphia, PA, USA.

Hauk, O. (2004). Keep it simple: a case for using classical minimum norm estimation in the analysis of EEG and MEG data. *NeuroImage*, 21(4):1612–1621.

Hill, R. A., Chiappa, K. H., Huang-Hellinger, F., and Jenkins, B. G. (1995). EEG during MR imaging: differentiation of movement artifact from paroxysmal cortical activity. *Neurology*, 45(10):1942–1943.

Hillebrand, A. and Barnes, G. R. (2003). The use of anatomical constraints with MEG beamformers. *NeuroImage*, 20(4):2302–2313.

Horn, B. K. P. (1987). Closed-form solution of absolute orientation using unit quaternions. *J. of Opt. Soc. Amer.*, 4(4):629–642.

Horn, B. K. P., Hilden, H., and Negahdaripour, S. (1988). Closed-form solution of absolute orientation using orthonormal matrices. *J. of Opt. Soc. Amer.*, 5(7):1127–1135.

Horovitz, S. G., Rossion, B., Skudlarski, P., and Gore, J. C. (2004). Parametric design and correlational analyses help integrating fMRI and electrophysiological data during face processing. *NeuroImage*, 22(4):1587–1595.

Horovitz, S. G., Skudlarski, P., and Gore, J. C. (2002). Correlations and dissociations between BOLD signal and P300 amplitude in an auditory oddball task: a parametric approach to combining fMRI and ERP. *Magn Reson Imaging*, 20(4):319–325.

Huang-Hellinger, F. R., Breiter, H. C., McCormack, G., Cohen, M. S., Kwong, K. K., Sutton, J. P., Savoy, R. L., Weisskoff, R. M., Davis, T. L., Baker, J. R., Belliveau, J. W., and Rosen, B. R. (1995). Simultaneous functional magnetic resonance imaging and electrophysiological recording. *Hum Brain Mapp*, 3:13–25.

Huppertz, H. J., Otte, M., Grimm, C., Kristeva-Feige, R., Mergner, T., and Lucking, C. H. (1998). Estimation of the accuracy of a surface matching technique for registration of EEG and MRI data. *Electroencephalogr Clin Neurophysiol*, 106(5):409–415.

Ives, J. R., Warach, S., Schmitt, F., Edelman, R. R., and Schomer, D. L. (1993). Monitoring the patient's EEG during echo planar MRI. *Electroencephalogr Clin Neurophysiol*, 87(6):417–420.

Jeffs, B., Leahy, R., and Singh, M. (1987). An evaluation of methods for neuromagnetic image reconstruction. *IEEE Trans Biomed Eng*, 34(9):713–723.

Jun, S. C. and Pearlmutter, B. A. (2005). Fast robust subject-independent magnetoencephalographic source localization using an artificial neural network. *Human Brain Mapping*, 24(1):21–34.

Jun, S. C., Pearlmutter, B. A., and Nolte, G. (2003). MEG source localization using a MLP with a distributed output representation. *IEEE Trans. Biomed. Eng.*, 50(6):786–789.

Jung, T.-P., Humphries, C., Lee, T.-W., Makeig, S., McKeown, M. J., Iragui, V., and Sejnowski, T. J. (1999a). Removing electroencephalographic artifacts: comparison between ICA and PCA. In *Neural Networks for Signal Processing VIII*. IEEE Press.

Jung, T.-P., Humphries, C., Lee, T.-W., McKeown, M. J., Iragui, V., Makeig, S., and Sejnowski, T. J. (2000a). Removing electroencephalographic artifacts by blind source separation. *Psychophysiology*, 37:163–178.

Jung, T.-P., Makeig, S., Westerfield, M., Townsend, J., Courchesne, E., and Sejnowski, T. J. (1999b). Analyzing and visualizing single-trial event-related potentials. In *Advances in Neural Info. Proc. Sys. 11*, pages 118–124. MIT Press.

Jung, T.-P., Makeig, S., Westerfield, M., Townsend, J., Courchesne, E., and Sejnowski, T. J. (2000b). Removal of eye activity artifacts from visual event-related potentials in normal and clinical subjects. *Clinical Neurophysiology*, 111(10):1745–1758.

Kober, H., Nimsky, C., Moller, M., Hastreiter, P., Fahlbusch, R., and Ganslandt, O. (2001). Correlation of sensorimotor activation with functional magnetic resonance imaging and magnetoencephalography in presurgical functional imaging: a spatial analysis. *NeuroImage*, 14(5):1214–1228.

Korvenoja, A., Huttunen, J., Salli, E., Pohjonen, H., Martinkauppi, S., Palva, J. M., Lauronen, L., Virtanen, J.,

Ilmoniemi, R. J., and Aronen, H. J. (1999). Activation of multiple cortical areas in response to somatosensory stimulation: combined magnetoencephalographic and functional magnetic resonance imaging. *Hum Brain Mapp*, 8(1):13–27.

Kozinska, D., Carducci, F., and Nowinski, K. (2001). Automatic alignment of EEG/MEG and MRI data sets. *Clin Neurophysiol*, 112(8):1553–1561.

Krakow, K., Allen, P. J., Symms, M. R., Lemieux, L., Josephs, O., and Fish, D. R. (2000). EEG recording during fMRI experiments: image quality. *Hum Brain Mapp*, 10(1):10–15.

Krakow, K., Lemieux, L., Messina, D., Scott, C. A., Symms, M. R., Duncan, J. S., and Fish, D. R. (2001). Spatio-temporal imaging of focal interictal epileptiform activity using EEG-triggered functional MRI. *Epileptic Disord*, 3(2):67–74.

Krakow, K., Wieshmann, U. C., Woermann, F. G., Symms, M. R., McLean, M. A., Lemieux, L., Allen, P. J., Barker, G. J., Fish, D. R., and Duncan, J. S. (1999a). Multimodal MR imaging: functional, diffusion tensor, and chemical shift imaging in a patient with localization-related epilepsy. *Epilepsia*, 40(10):1459–1462.

Krakow, K., Woermann, F. G., Symms, M. R., Allen, P. J., Lemieux, L., Barker, G. J., Duncan, J. S., and Fish, D. R. (1999b). EEG-triggered functional MRI of interictal epileptiform activity in patients with partial seizures. *Brain*, 122(9):1679–1688.

Kruggel, F., Herrmann, C. S., Wiggins, C. J., and von Cramon, D. Y. (2001). Hemodynamic and electroencephalographic responses to illusory figures: recording of the evoked potentials during functional MRI. *NeuroImage*, 14(6):1327–1336.

Kruggel, F., Wiggins, C. J., Herrmann, C. S., and von Cramon, D. Y. (2000). Recording of the event-related potentials during functional MRI at 3.0 Tesla field strength. *Magn Reson Med*, 44(2):277–282.

Lagerlund, T. D., Sharbrough, F. W., Jack, Jr, C. R., Erickson, B. J., Strelow, D. C., Cicora, K. M., and Busacker, N. E. (1993). Determination of 10-20 system electrode locations using magnetic resonance image scanning with markers. *Electroencephalogr Clin Neurophysiol*, 86(1):7–14.

Lahaye, P.-J., Baillet, S., Poline, J.-B., and Garnero, L. (2004). Fusion of simultaneous fMRI/EEG data based on the electro-metabolic coupling. In *Proc. IEEE ISBI*, pages 864–867, Arlington, Virginia.

Lamm, C., Windischberger, C., Leodolter, U., Moser, E., and Bauer, H. (2001). Co-registration of EEG and MRI data using matching of spline interpolated and MRI-segmented reconstructions of the scalp surface. *Brain Topogr*, 14(2):93–100.

Lange, N. and Zeger, S. L. (1997). Non-linear fourier time series analysis for human brain mapping by functional magnetic resonance imaging. *Appl. Stat.*, 46(1):1–29.

Lantz, G., Spinelli, L., Menendez, R. G., Seeck, M., and Michel, C. M. (2001). Localization of distributed sources and comparison with functional MRI. *Epileptic Disord*, Special Issue:45–58.

Laufs, H., Kleinschmidt, A., Beyerle, A., Eger, E., Salek-Haddadi, A., Preibisch, C., and Krakow, K. (2003a). EEG-correlated fMRI of human alpha activity. *NeuroImage*, 19(4):1463–1476.

Laufs, H., Krakow, K., Sterzer, P., Eger, E., Beyerle, A., Salek-Haddadi, A., and Kleinschmidt, A. (2003b). Electroencephalographic signatures of attentional and cognitive default modes in spontaneous brain activity fluctuations at rest. *Proc Natl Acad Sci U S A*, 100(19):11053–11058.

Lawson, C. L. and Hanson, R. J. (1974). *Solving Least Squares Problems*. Series in Automatic Computation. Prentice-Hall, Englewood Cliffs, NJ 07632, USA.

Lazeyras, F., Blanke, O., Perrig, S., Zimine, I., Golay, X., Delavelle, J., Michel, C. M., de Tribolet, N., Villemure, J. G., and Seeck, M. (2000). EEG-triggered functional MRI in patients with pharmacoresistant epilepsy. *J Magn Reson Imaging*, 12(1):177–185.

Lazeyras, F., Zimine, I., Blanke, O., Perrig, S. H., and Seeck, M. (2001). Functional MRI with simultaneous EEG recording: feasibility and application to motor and visual activation. *J Magn Reson Imaging*, 13(6):943–948.

Leahy, R. M., Baillet, S., and Mosher, J. C. (2004). Integrated matlab toolbox dedicated to magnetoencephalog-

raphy (MEG) and electroencephalography (EEG) data visualization and processing.

Lemieux, L., Allen, P. J., Franconi, F., Symms, M. R., and Fish, D. R. (1997). Recording of EEG during fMRI experiments: patient safety. *Magn Reson Med*, 38(6):943–952.

Lemieux, L., Krakow, K., and Fish, D. R. (2001). Comparison of spike-triggered functional MRI BOLD activation and EEG dipole model localization. *NeuroImage*, 14(5):1097–1104.

Liebenthal, E., Ellingson, M. L., Spanaki, M. V., Prieto, T. E., Ropella, K. M., and Binder, J. R. (2003). Simultaneous ERP and fMRI of the auditory cortex in a passive oddball paradigm. *NeuroImage*, 19(4):1395–1404.

Liu, A. K., Belliveau, J. W., and Dale, A. M. (1998). Spatiotemporal imaging of human brain activity using functional MRI constrained magnetoencephalography data: Monte Carlo simulations. *Proc Natl Acad Sci U S A*, 95(15):8945–8950.

Logothetis, N. K. and Wandell, B. A. (2004). Interpreting the BOLD signal. *Annu Rev Physiol*, 66:735–769.

Makiranta, M. J., Ruohonen, J., Suominen, K., Sonkajarvi, E., Salomaki, T., Kiviniemi, V., Seppanen, T., Alahuhta, S., Jantti, V., and Tervonen, O. (2004). BOLD-contrast functional MRI signal changes related to intermittent rhythmic delta activity in EEG during voluntary hyperventilation-simultaneous EEG and fMRI study. *NeuroImage*, 22(1):222–231.

Malmivuo, J. and Plonsey, R. (1995). *Bioelectromagnetism—Principles and Applications of Bioelectric and Biomagnetic Fields*. Oxford University Press, New York, 1995.

Malmivuo, J., Suihko, V., and Eskola, H. (1997). Sensitivity distributions of EEG and MEG measurements. *IEEE Trans Biomed Eng*, 44(3):196–208.

Marin, G., Guerin, C., Baillet, S., Garnero, L., and Meunier, G. (1998). Influence of skull anisotropy for the forward and inverse problems in EEG: simulation studies using FEM on realistic head models. *Hum. Brain. Mapp.*, 6:250–269.

Marrelec, G., Benali, H., Ciuciu, P., Pelegrini-Issac, M., and Poline, J. B. (2003). Robust Bayesian estimation of the hemodynamic response function in event-related BOLD fMRI using basic physiological information. *Hum Brain Mapp*, 19(1):1–17.

Martinez-Montes, E., Valdes-Sosa, P. A., Miwakeichi, F., Goldman, R. I., and Cohen, M. S. (2004). Concurrent EEG/fMRI analysis by multiway Partial Least Squares. *NeuroImage*, 22(3):1023–1034.

McKeown, M. J., Makeig, S., Brown, G. G., Jung, T.-P., Kindermann, S. S., Bell, A. J., and Sejnowski, T. J. (1998). Analysis of fMRI data by blind separation into independent spatial components. *Human Brain Mapping*, 6:160–188.

Melie-García, L., Trujillo-Barreto, N. J., Martínez-Montes, E., Koenig, T., and Valdés-Sosa, P. A. (2004). EEG imaging via BMA with fMRI pre-defined prior model probabilities. In *Hum. Brain. Mapp.*, Budapest, Hungary.

Menon, V., Ford, J. M., Lim, K. O., Glover, G. H., and Pfefferbaum, A. (1997). Combined event-related fMRI and EEG evidence for temporal-parietal cortex activation during target detection. *Neuroreport*, 8(14):3029–3037.

Michel, C. M., Murray, M. M., Lantz, G., Gonzalez, S., Spinelli, L., and Grave De Peralta, R. (2004). EEG source imaging. *Clin Neurophysiol*, 115(10):2195–2222.

Miller, C. E. and Henriquez, C. S. (1990). Finite element analysis of bioelectric phenomena. *Crit Rev Biomed Eng*, 18(3):207–233.

Moosmann, M., Ritter, P., Krastel, I., Brink, A., Thees, S., Blankenburg, F., Taskin, B., Obrig, H., and Villringer, A. (2003). Correlates of alpha rhythm in functional magnetic resonance imaging and near infrared spectroscopy. *NeuroImage*, 20(1):145–158.

Moran, J. E. (2005). MEG tools for Matlab software.

Mosher, J. C., Leahy, R. M., and Lewis, P. S. (1999). EEG and MEG: Forward solutions for inverse methods. *IEEE Trans. Biomed. Eng.*, 46(3):245–260.

Mulert, C., Jager, L., Schmitt, R., Bussfeld, P., Pogarell, O., Moller, H. J., Juckel, G., and Hegerl, U. (2004). Integration of fMRI and simultaneous EEG: towards a comprehensive understanding of localization and time-

course of brain activity in target detection. *NeuroImage*, 22(1):83–94.

Murakami, S., Hirose, A., and Okada, Y. (2003). Contribution of ionic currents to magnetoencephalography (MEG) and electroencephalography (EEG) signals generated by guinea-pig CA3 slices. *J Physiol*, 553(Pt 3):975–985.

Negishi, M., Abildgaard, M., Nixon, T., and Todd Constable, R. (2004). Removal of time-varying gradient artifacts from EEG data acquired during continuous fMRI. *Clin Neurophysiol*, 115(9):2181–2192.

NeuroFEM (2005). Finite element software for fast computation of the forward solution in EEG/MEG source localisation. Max Planck Institute for Human Cognitive and Brain Sciences.

Niedermeyer, E. (1997). Alpha rhythms as physiological and abnormal phenomena. *Int J Psychophysiol*, 26(1-3):31–49.

Nielsen, F. Å. (2001). Bibliography of segmentation in neuroimaging.

Nolte, G. (2003). The magnetic lead field theorem in the quasi-static approximation and its use for magnetoencephalography forward calculation in realistic volume conductors. *Phys. Med. Biol.*, 48:3637–3652.

Nolte, G. (2004). The magnetic lead field theorem in the quasi-static approximation and its use for MEG forward calculation in realistic volume conductors. *Physics in Medicine and Biology*, 48(22):3637–3652.

Nunez, P. L. (1981). *Electric Fields of the Brain: The Neurophysics of EEG*. New York: Oxford University Press.

Nunez, P. L. and Silberstein, R. B. (2000). On the relationship of synaptic activity to macroscopic measurements: does co-registration of EEG with fMRI make sense? *Brain Topogr*, 13(2):79–96.

Okada, Y., Lahteenmaki, A., and Xu, C. (1999). Comparison of MEG and EEG on the basis of somatic evoked responses elicited by stimulation of the snout in the juvenile swine. *Clin Neurophysiol*, 110(2):214–229.

Pascual-Marqui, R. D., Michel, C. M., and Lehman, D. (1994). Low resolution electromagnetic tomography: A new method for localizing electrical activity of the brain. *Int. J. of Psychophysiol.*, 18:49–65.

Paulesu, R. S., Frackowiak, R. S. J., and Bottini, G. (1997). Maps of somatosensory systems. In Frackowiak, R. S. J., editor, *Human brain function*, page 528. Academic Press, San Diego, CA.

Phillips, C., Rugg, M. D., and Friston, K. J. (2002a). Anatomically informed basis functions for EEG source localization: combining functional and anatomical constraints. *NeuroImage*, 16(3.1):678–695.

Phillips, C., Rugg, M. D., and Friston, K. J. (2002b). Systematic regularization of linear inverse solutions of the EEG source localization problem. *NeuroImage*, 17(1):287–301.

Poupon, F. (1999). *Parcellisation systématique du cerveau en volumes d'intérêt. Le cas des structures profondes*. Phd thesis, INSA Lyon, Lyon, France.

Pruis, G. W., Gilding, B. H., and Peters, M. J. (1993). A comparison of different numerical methods for solving the forward problem in EEG and MEG. *Physiol Meas*, 14 Suppl 4A:A1–9.

Rajapakse, J. C., Kruggel, F., Maisog, J. M., and von Cramon, D. Y. (1998). Modeling hemodynamic response for analysis of functional MRI time-series. *Hum Brain Mapp*, 6(4):283–300.

Robinson, S. E. and Vrba, J. (1999). Functional neuroimaging by syntheticaperture magnetometry (SAM). In Yoshimoto, T., Kotani, M., Kuriki, S., Karibe, H., and Nakasato, N., editors, *Recent Advances in Biomagnetism*, pages 302–305, Sendai, Japan. Tohoku Univ. Press.

Sahani, M. and Nagarajan, S. S. (2004). Reconstructing MEG sources with unknown correlations. In *Advances in Neural Info. Proc. Sys. 16*. MIT Press.

Saleheen, H. I. and Ng, K. T. (1997). New finite difference formulations for general inhomogeneous anisotropic bioelectric problems. *IEEE Trans Biomed Eng*, 44(9):800–809.

Salek-Haddadi, A., Friston, K. J., Lemieux, L., and Fish, D. R. (2003). Studying spontaneous EEG activity with fMRI. *Brain Res Brain Res Rev*, 43(1):110–133.

Salek-Haddadi, A., Merschhemke, M., Lemieux, L., and Fish, D. R. (2002). Simultaneous EEG-Correlated Ictal fMRI. *NeuroImage*, 16(1):32–40.

Schmidt, D. M., George, J. S., and Wood, C. C. (1999). Bayesian inference applied to the electromagnetic inverse

problem. *Hum. Brain. Mapp.*, 7(3):195–212.

Schomer, D. L., Bonmassar, G., Lazeyras, F., Seeck, M., Blum, A., Anami, K., Schwartz, D., Belliveau, J. W., and Ives, J. (2000). EEG-Linked functional magnetic resonance imaging in epilepsy and cognitive neurophysiology. *J Clin Neurophysiol*, 17(1):43–58.

Schulz, M., Chau, W., Graham, S. J., McIntosh, A. R., Ross, B., Ishii, R., and Pantev, C. (2004). An integrative MEG-fMRI study of the primary somatosensory cortex using cross-modal correspondence analysis. *NeuroImage*, 22(1):120–133.

Schwartz, D. P., Poiseau, E., Lemoine, D., and Barillot, C. (1996). Registration of MEG/EEG data with 3D MRI: Methodology and precision issues. *Brain Topogr.*, 9(1):101–116.

SCIRun (2002). SCIRun: a scientific computing problem solving environment. Scientific Computing and Imaging Institute (SCI).

Seeck, M., Lazeyras, F., Michel, C. M., Blanke, O., Gericke, C. A., Ives, J., Delavelle, J., Golay, X., Haenggeli, C. A., de Tribolet, N., and Landis, T. (1998). Non-invasive epileptic focus localization using EEG-triggered functional MRI and electromagnetic tomography. *Electroencephalogr Clin Neurophysiol*, 106(6):508–512.

Seiyama, A., Seki, J., Tanabe, H. C., Sase, I., Takatsuki, A., Miyauchi, S., Eda, H., Hayashi, S., Imaruoka, T., Iwakura, T., and Yanagida, T. (2004). Circulatory basis of fMRI signals: relationship between changes in the hemodynamic parameters and BOLD signal intensity. *NeuroImage*, 21(4):1204–1214.

Shattuck, D. and Leahy, R. (2002). BrainSuite: an automated cortical surface identification tool. *Med Image Anal*, 6(2):129–142.

Sijbers, J., Michiels, I., Verhoye, M., Van Audekerke, J., Van der Linden, A., and Van Dyck, D. (1999). Restoration of MR-induced artifacts in simultaneously recorded MR/EEG data. *Magn Reson Imaging*, 17(9):1383–1391.

Sijbers, J., Vanrumste, B., Van Hoey, G., Boon, P., Verhoye, M., Van der Linden, A., and Van Dyck, D. (2000). Automatic localization of EEG electrode markers within 3D MR data. *Magn Reson Imaging*, 18(4):485–488.

Singh, K. D., Barnes, G. R., Hillebrand, A., Forde, E. M., and Williams, A. L. (2002). Task-related changes in cortical synchronization are spatially coincident with the hemodynamic response. *NeuroImage*, 16(1):103–114.

Singh, K. D., Holliday, I. E., Furlong, P. L., and Harding, G. F. (1997). Evaluation of MRI-MEG/EEG co-registration strategies using Monte Carlo simulation. *Electroencephalogr Clin Neurophysiol*, 102(2):81–85.

Singh, M., Kim, S., and Kim, T. S. (2003). Correlation between BOLD-fMRI and EEG signal changes in response to visual stimulus frequency in humans. *Magn Reson Med*, 49(1):108–114.

Soltysik, D. A., Peck, K. K., White, K. D., Crosson, B., and Briggs, R. W. (2004). Comparison of hemodynamic response nonlinearity across primary cortical areas. *NeuroImage*, 22(3):1117–1127.

Sommer, M., Meinhardt, J., and Volz, H. P. (2003). Combined measurement of event-related potentials (ERPs) and fMRI. *Acta Neurobiol Exp (Wars)*, 63(1):49–53.

Srivastava, G., Crottaz-Herbette, S., Lau, K., Glover, G., and Menon, V. (2005). ICA-based procedures for removing ballistocardiogram artifacts from EEG data acquired in the MRI scanner. *Neuroimage*, 24(1):50–60.

Stefanovic, B., Warnking, J. M., and Pike, G. B. (2004). Hemodynamic and metabolic responses to neuronal inhibition. *NeuroImage*, 22(2):771–778.

Tang, A. C. and Pearlmutter, B. A. (2003). Independent components of magnetoencephalography: Localization and single-trial response onset detection. In Lu, Z.-L. and Kaufman, L., editors, *Magnetic Source Imaging of the Human Brain*, pages 159–201. Lawrence Erlbaum Associates.

Tang, A. C., Pearlmutter, B. A., Zibulevsky, M., and Carter, S. A. (2000a). Blind separation of multichannel neuromagnetic responses. *Neurocomputing*, 32–33:1115–1120.

Tang, A. C., Pearlmutter, B. A., Zibulevsky, M., Hely, T. A., and Weisend, M. P. (2000b). An MEG study of response latency and variability in the human visual system during a visual-motor integration task. In *Advances in Neural Info. Proc. Sys. 12*, pages 185–191. MIT Press.

Towle, V. L., Bolanos, J., Suarez, D., Tan, K., Grzeszczuk, R., Levin, D. N., Cakmur, R., Frank, S. A., and Spire, J. P. (1993). The spatial location of EEG electrodes: locating the best-fitting sphere relative to cortical anatomy. *Electroencephalogr Clin Neurophysiol*, 86(1):1–6.

Trujillo-Barreto, N. J., Aubert-Vazquez, E., and Valdes-Sosa, P. A. (2004). Bayesian model averaging in EEG/MEG imaging. *NeuroImage*, 21(4):1300–1319.

Trujillo-Barreto, N. J., Martínez-Montes, E., Melie-García, L., and Valdés-Sosa, P. A. (2001). A symmetrical bayesian model for fMRI and EEG/MEG Neuroimage fusion. *Int. J. of Bioelectromag.*, 3(1).

Tuch, D. S., Wedeen, V. J., Dale, A. M., George, J., and Belliveau, J. W. (2001). Conductivity tensor mapping of the human brain using diffusion tensor MRI. *Proc Natl Acad Sci U S A*, 98(20):11697–11701.

Van Essen, D. (2004). Surface reconstruction by filtering and intensity transformations.

Van Veen, B. D., van Drongelen, W., Yuchtman, M., and Suzuki, A. (1997). Localization of brain electrical activity via linearly constrained minimum variance spatial filtering. *IEEE Trans Biomed Eng*, 44(9):867–880.

Vanhatalo, S., Tallgren, P., Becker, C., Holmes, M. D., Miller, J. W., Kaila, K., and Voipio, J. (2003). Scalp-recorded slow EEG responses generated in response to hemodynamic changes in the human brain. *Clin Neurophysiol*, 114(9):1744–1754.

Vanni, S., Warnking, J., Dojat, M., Delon-Martin, C., Bullier, J., and Segebarth, C. (2004). Sequence of pattern onset responses in the human visual areas: an fMRI constrained VEP source analysis. *NeuroImage*, 21(3):801–817.

Vigário, R., Särelä, J., Jousmäki, V., Hämäläinen, M., and Oja, E. (2000). Independent component approach to the analysis of EEG and MEG recordings. *IEEE Trans. Biomed. Eng.*, 47(5):589–593.

Vitacco, D., Brandeis, D., Pascual-Marqui, R., and Martin, E. (2002). Correspondence of event-related potential tomography and functional magnetic resonance imaging during language processing. *Hum Brain Mapp*, 17(1):4–12.

Vrba, J. and Robinson, S. E. (2000). Differences between Synthetic Aperture Magnetometry (SAM) and linear beamformers. In Nenonen, J., Ilmoniemi, R., and Katila, T., editors, *12th Int Conf Biomagnet*, 12th International Conference on Biomagnetism, Helsinki, Finland. Biomag2000.

Vrba, J. and Robinson, S. E. (2001). Signal processing in magnetoencephalography. *Methods*, 25(2):249–271.

Wagner, M. and Fuchs, M. (2001). Integration of functional MRI, structural MRI, EEG, and MEG. *Int. J. of Bioelectromag.*, 3(1).

Waites, A., Shaw, M., Briellmann, R., Labate, A., Abbott, D., and Jackson, G. (2005). How reliable are fMRI-EEG studies of epilepsy? A nonparametric approach to analysis validation and optimization. *Neuroimage*, 24(1):192–199.

Wang, J. Z., Williamson, S. J., and Kaufman, L. (1992). Magnetic source images determined by a lead-field analysis: the unique minimum-norm least-squares estimation. *IEEE Trans. Biomed. Eng.*, 39(7):665–675.

Warach, S., Ives, J. R., Schlaug, G., Patel, M. R., Darby, D. G., Thangaraj, V., Edelman, R. R., and Schomer, D. L. (1996). EEG-triggered echo-planar functional MRI in epilepsy. *Neurology*, 47(1):89–93.

Weber, D. (2004). EEG and MRI Matlab toolbox.

Wieringa, H. J., Peters, M. J., and Lopes da Silva, F. (1993). The estimation of a realistic localization of dipole layers within the brain based on functional (EEG, MEG) and structural (MRI) data: a preliminary note. *Brain Topogr*, 5(4):327–330.

Wikswo, Jr, J. P., Gevins, A., and Williamson, S. J. (1993). The future of the EEG and MEG. *Electroencephalogr Clin Neurophysiol*, 87(1):1–9.

Wolters, C. H., Anwander, A., Koch, M. A., Reitzinger, S., Kuhn, M., and Svensén, M. (2001). Influence of head tissue conductivity anisotropy on human EEG and meg using fast high resolution finite element modeling, based on a parallel algebraic multigrid solver. In Plesser, T. and Wittenburg, P., editors, *Forschung und wissenschaftliches Rechnen*, pages 111–157. Max-Planck-Gesselschaft, München.

Xiong, J., Fox, P. T., and Gao, J. H. (2003). Directly mapping magnetic field effects of neuronal activity by magnetic resonance imaging. *Hum Brain Mapp*, 20(1):41–49.

Zhang, Z. (1995). A fast method to compute surface potentials generated by dipoles within multilayer anisotropic spheres. *Phys. Med. Biol.*, 40:335–349.